
# NAVAL POSTGRADUATE SCHOOL

**MONTEREY, CALIFORNIA**

# THESIS

**OPTIMIZATION OF THE NPS TRANSONIC COMPRESSOR RIG DOWNSTREAM PRESSURE AND TEMPERATURE INSTRUMENTATION**

by

Taylor M. Adams

June 2023

Thesis Advisor: Walter C. Smith
Co-Advisors: Garth V. Hobson
Anthony J. Gannon

THIS PAGE INTENTIONALLY LEFT BLANK

| REPORT DOCUMENTATION PAGE | *Form Approved OMB No. 0704-0188* |
|---|---|



| **1. AGENCY USE ONLY** *(Leave blank)* | **2. REPORT DATE** June 2023 | **3. REPORT TYPE AND DATES COVERED** Master's thesis |
|---|---|---|

**4. TITLE AND SUBTITLE**
OPTIMIZATION OF THE NPS TRANSONIC COMPRESSOR RIG DOWNSTREAM PRESSURE AND TEMPERATURE INSTRUMENTATION

**5. FUNDING NUMBERS**

**6. AUTHOR(S)** Taylor M. Adams

**7. PERFORMING ORGANIZATION NAME(S) AND ADDRESS(ES)**
Naval Postgraduate School
Monterey, CA 93943-5000

**8. PERFORMING ORGANIZATION REPORT NUMBER**

**9. SPONSORING / MONITORING AGENCY NAME(S) AND ADDRESS(ES)**
N/A

**10. SPONSORING / MONITORING AGENCY REPORT NUMBER**

**11. SUPPLEMENTARY NOTES** The views expressed in this thesis are those of the author and do not reflect the official policy or position of the Department of Defense or the U.S. Government.

**12a. DISTRIBUTION / AVAILABILITY STATEMENT**
Approved for public release. Distribution is unlimited.

**12b. DISTRIBUTION CODE**
A

**13. ABSTRACT (maximum 200 words)**

In order to provide the fleet with the most beneficial research on military fan engines, the NPS Turbopropulsion Lab (TPL) required a modernization of its transonic compressor rig's (TCR) pressure and temperature instrumentation. An entirely new casing was designed and additively manufactured to provide a consistent datum for which new pressure and temperature rake probes could be designed and additively manufactured. This resulted in a more accurate and repeatable solution to map the internal characteristics of the rig. To optimize the instrumentation, a computational fluid dynamics (CFD) analysis was completed on the stator for the first time. Next, the CFD results guided the new design for the pressure and temperature probes by identifying the most effective measurement locations. In all, the TPL, and the Navy, will benefit for years to come as the TCR at NPS will provide more accurate and repeatable measurements on military fan engines.

**14. SUBJECT TERMS**
transonic compressor, instrumentation, stator casing, design, LDV plug, thermocouple, Kiel probe, 3D printing

**15. NUMBER OF PAGES**
99

**16. PRICE CODE**

| **17. SECURITY CLASSIFICATION OF REPORT** | **18. SECURITY CLASSIFICATION OF THIS PAGE** | **19. SECURITY CLASSIFICATION OF ABSTRACT** | **20. LIMITATION OF ABSTRACT** |
|---|---|---|---|
| Unclassified | Unclassified | Unclassified | UU |

NSN 7540-01-280-5500

Standard Form 298 (Rev. 2-89)
Prescribed by ANSI Std. 239-18

THIS PAGE INTENTIONALLY LEFT BLANK

**Approved for public release. Distribution is unlimited.**

# OPTIMIZATION OF THE NPS TRANSONIC COMPRESSOR RIG DOWNSTREAM PRESSURE AND TEMPERATURE INSTRUMENTATION

Taylor M. Adams
Ensign, United States Navy
BS, University of Washington, 2022

Submitted in partial fulfillment of the
requirements for the degree of

**MASTER OF SCIENCE IN AEROSPACE ENGINEERING**

from the

**NAVAL POSTGRADUATE SCHOOL**
**June 2023**

Approved by: Walter C. Smith
Advisor

Garth V. Hobson
Co-Advisor

Anthony J. Gannon
Co-Advisor

Brian S. Bingham
Chair, Department of Mechanical and Aerospace Engineering

THIS PAGE INTENTIONALLY LEFT BLANK

# ABSTRACT

In order to provide the fleet with the most beneficial research on military fan engines, the NPS Turbopropulsion Lab (TPL) required a modernization of its transonic compressor rig's (TCR) pressure and temperature instrumentation. An entirely new casing was designed and additively manufactured to provide a consistent datum for which new pressure and temperature rake probes could be designed and additively manufactured. This resulted in a more accurate and repeatable solution to map the internal characteristics of the rig. To optimize the instrumentation, a computational fluid dynamics (CFD) analysis was completed on the stator for the first time. Next, the CFD results guided the new design for the pressure and temperature probes by identifying the most effective measurement locations. In all, the TPL, and the Navy, will benefit for years to come as the TCR at NPS will provide more accurate and repeatable measurements on military fan engines.

THIS PAGE INTENTIONALLY LEFT BLANK

# TABLE OF CONTENTS

# LIST OF FIGURES

THIS PAGE INTENTIONALLY LEFT BLANK

# LIST OF TABLES

THIS PAGE INTENTIONALLY LEFT BLANK

# LIST OF ACRONYMS AND ABBREVIATIONS

| | |
|---|---|
| AM | additive manufacturing |
| CAD | computer-aided design |
| CFD | computational fluid dynamics |
| COTS | commercial off the shelf |
| DUMI | datum universal measurement insert |
| IGV | inlet guide vane |
| LDV | laser Doppler velocimetry |
| NPS | Naval Postgraduate School |
| NPSMF | Naval Postgraduate School Military Fan |
| SST | shear stress transport |
| TPL | Turbopropulsion Laboratory |

THIS PAGE INTENTIONALLY LEFT BLANK

# ACKNOWLEDGMENTS

I want to begin by giving credit and expressing gratitude to my advisors, Dr. Walter Smith, Dr. Anthony Gannon, and Dr. Garth Hobson, for their valuable guidance throughout my research project. They went above and beyond to help me learn and achieve more than I thought possible. While they presented me with challenges, they also supported me every step of the way. Most significantly, they encouraged me to take responsibility for my learning, a lesson that will stay with me as I progress in my future endeavors.

I would also like to express my gratitude to my classmates for their assistance and encouragement. Meeting colleagues at NPS has been one of my most cherished experiences, and I consider myself fortunate to have them as my friends.

Next, I want to acknowledge the additional faculty members at NPS who graciously shared their knowledge and expertise with me. This includes all of my professors, as well as John Mobley and Doug Seivwright. Each of them unselfishly imparted their knowledge to assist me in attaining my goals.

Most of all, I couldn't have done any of this without the love and support from my friends and family. My family has always been my bedrock and my source of strength. It's been a challenging year to say the least, but there's no one else I'd rather have in my corner.

THIS PAGE INTENTIONALLY LEFT BLANK

# I. INTRODUCTION

The Turbopropulsion Laboratory (TPL) is located at the Naval Postgraduate School (NPS) in Monterey, CA. The TPL operates within the Department of Mechanical and Aerospace Engineering. Various branches of the Department of Defense frequently fund research projects at the TPL to explore technology that could benefit the Navy or the military in general.

One of the primary areas of research at the TPL is the NPS military fan (NPSMF), which is a scaled replica of a modern military turbofan engine. The primary focus of research in recent times at the TPL has been on the transonic compressor rig (TCR) with most of it aiming to identify methods of improving the stall margin in turbofan engines. The NPSMF was procured in 2010 and first tested by McNab in 2011 [1] and has been consistently researched and enhanced since then [2]. A computer-aided design (CAD) model of the TCR was provided in Figure 1 to display a section view of the TCR, which depicts the flow path from right to left. The first components encountered by the flow are the inlet guide vanes (IGVs), shown in green in Figure 1, which guide the flow into the rotor. As the flow passes through the rotor, it gains velocity and pressure due to the rotational force created by the blades. However, this rotational flow needs to be straightened out to be discharged axially from the rig, hence the need for stator blades which help redirect the flow to move in a more axial direction. After passing through the stator blades, the flow encounters a casing containing pressure and temperature instrumentation. This instrumentation is crucial for measuring the performance of the rig. This study seeks to improve the instrumentation at the downstream casing location.

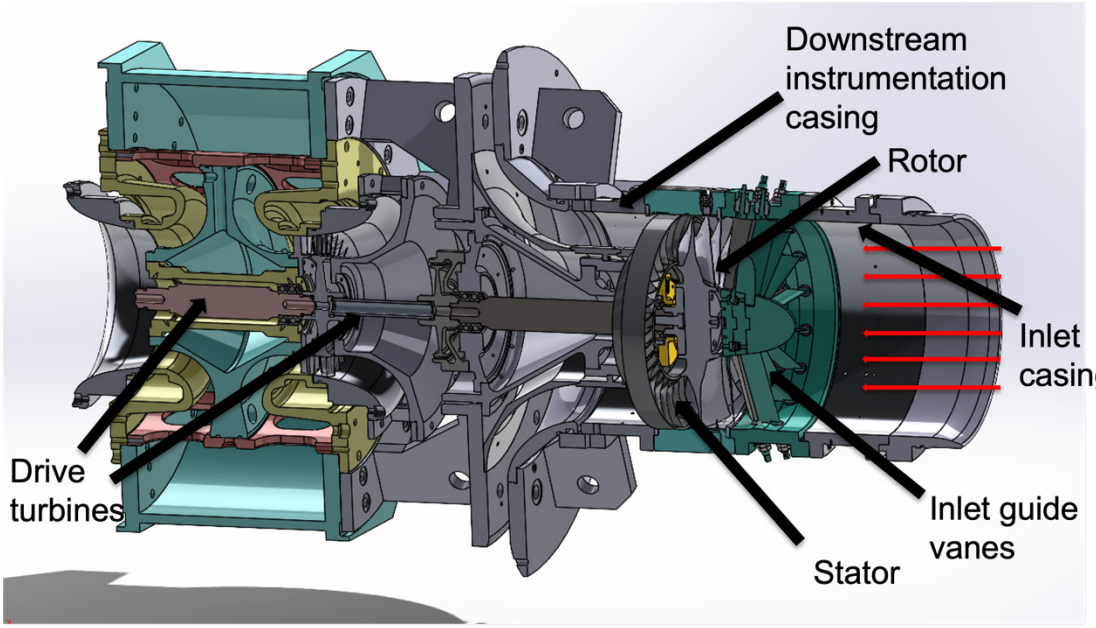


Figure 1. Section view of a CAD model of the TCR.

## A. MOTIVATION

The TPL constantly seeks to take advantage of new technologies to enhance instrumentation on the TCR. Prior to this work, the instrumentation on the TCR was standard fan performance instrumentation. One such technology that has not been taken advantage of has been metal additive manufacturing which would allow for customizable pressure and temperature probe measurements for each test configuration. The existing instrumentation exhibited limitations, including maintaining numerous measurement configurations, lacking redundancy, possessing limited design flexibility, and requiring excessive maintenance, as evidenced by Figure 2. To address these issues and improve the effectiveness of the instrumentation, the TPL undertook a redesign project. This report presents the design considerations, methodology, and implementation of a new casing that securely holds individual pressure and temperature rake probes. Additionally, the casing was designed to accommodate future additively manufactured instrumentation rakes using the in-house EOS M 100 3D printer, a powder bed fusion metal printer with a build size of approximately 10 cm x 10 cm x 9.5 cm (3.94 in x 3.94 in x 3.74 in) capable of printing in titanium. The results demonstrate significant improvements in accuracy, repeatability, and user-friendliness of the instrumentation system.

Figure 2. Existing outlet instrumentation.

It is not possible to understand what happens within the TCR without taking measurements. Furthermore, without effective measurements, it is impossible to determine how to enhance the TCR. Therefore, this thesis aimed to provide an accurate, repeatable, useful, and user-friendly solution to improve the measurement of TCR characteristics. Quality measurements were critical not only to identify how to enhance the TCR, but also to guarantee its safe operation. Pressure and temperature measurements were necessary to calculate other essential parameters, including efficiency, mass flow rates, and pressure ratios. Inaccurate measurements could result in either incorrect recommendations for improvement or unsafe operation of the TCR. Therefore, precise and reliable measurements were vital to ensure both optimal performance and safety.

## B. LITERATURE REVIEW

To design an effective solution, it was imperative to understand the context of the situation. As a result, several topics that would be beneficial to understand throughout the duration of the project were researched, analyzed, and reported on. These topics included common instrumentation types used on transonic compressors, the use of computational fluid dynamics (CFD), current trends in additive manufacturing, and the capabilities of the in-house EOS M100 3D metal printer. The insights gained from this research provided valuable guidance for developing solutions for the rest of the project.

### 1. Common Instrumentation Practices in Transonic Compressors

Several types of instrumentation are commonly used on transonic compressors, such as Kiel probes, fast-response thermocouples, hot-wire anemometers, and laser Doppler velocimeters (LDVs). Currently, the TCR employs a combination of Kiel probes and Kiel probe/thermocouple combination probes at different locations around the rig to measure and analyze the flow characteristics, as seen in Figure 3.

Figure 3. Internal view of the TCR instrumentation. Source: [3].

The most common type of instrumentation used on the NPS TCR is the Kiel probe. This device is highly effective in measuring a flow's total, or stagnation, pressure by bringing the flow to a standstill nearly isentropically and recording its pressure. Figure 3 displays how the instrumentation is currently set on the rig with the Kiel probes and the Kiel probe/thermocouple combinations protruding into the flow field. One significant advantage of the Kiel probe design is its ability to measure pressure over a wide range of flow angles. Typically, a conical gas path is incorporated into the probe leading to a pressure sensor that measures pressure. Essentially, the Kiel probe is a way to house a Pitot tube, which is shown in Figure 4, to measure the stagnation pressure of a location [4]. As depicted in Figure 5 and Figure 6, Kiel probes may be arranged in a "rake" configuration, where they are stacked on top of each other. This arrangement enables multiple measurements to be taken at different radial positions with the same axial and circumferential position while reducing the number of penetrations and blockages required to obtain the same number of measurements.

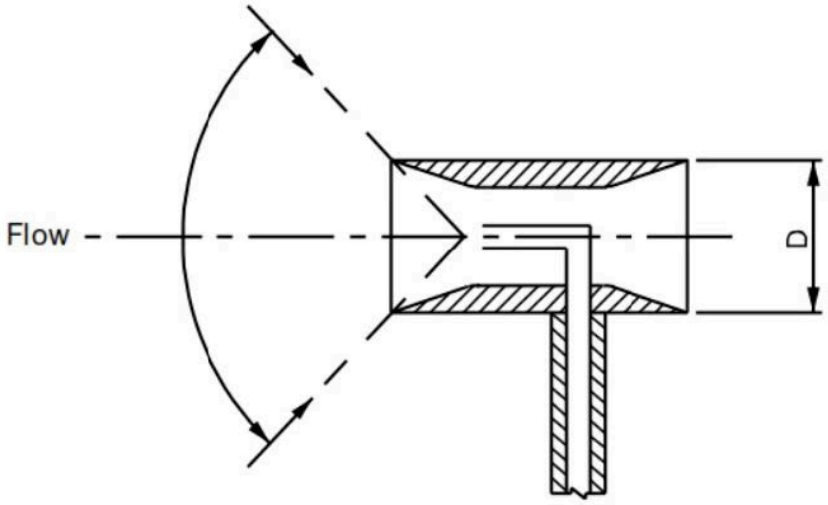


Figure 4. Side view diagram of how Kiel probes work. Source: [5].

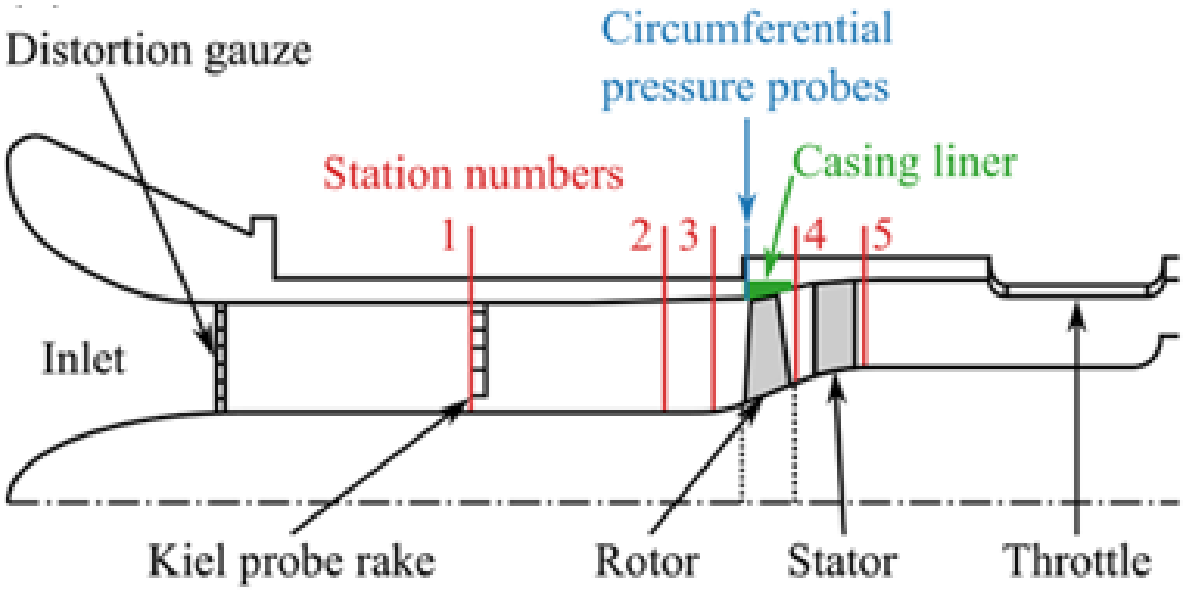


Figure 5. Diagram of the Kiel probe's role in a turbofan engine. Source: [6].

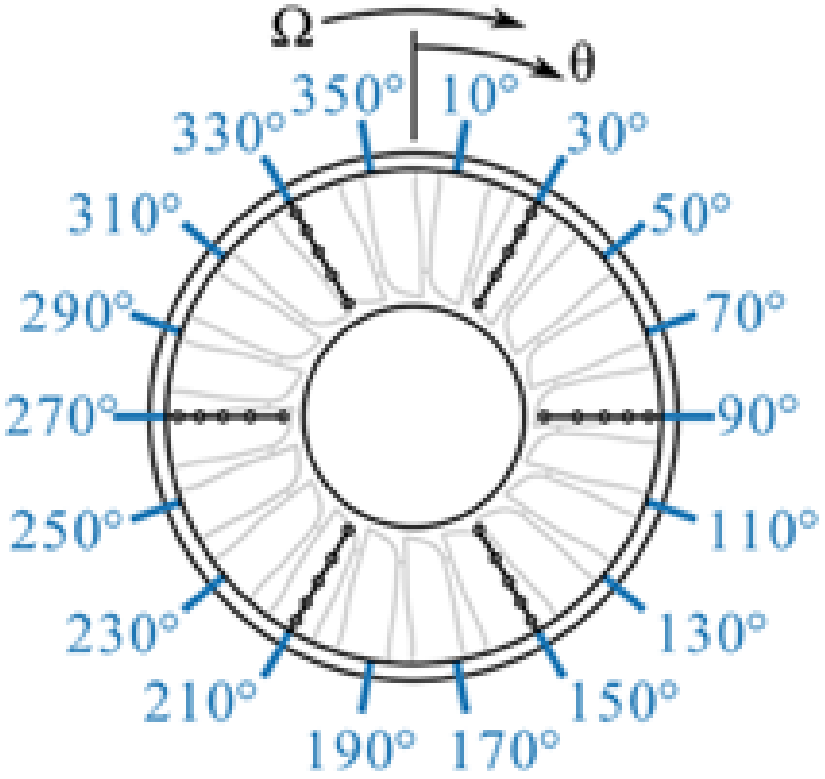


Figure 6. Diagram of circumferential Kiel probe rake placement in a turbofan engine. Source: [6].

Another form of instrumentation commonly found on the NPS TCR is thermocouples. Thermocouples usually consist of a metal tube that houses two wires of different metal types exposed at a joining point, as Figure 7 illustrates. This junction of different metals creates a thermoelectric voltage difference between ends depending on the temperature. With this known voltage, the thermocouple can be calibrated to read out the temperature according to the change in voltage difference. As a result, thermocouples are an accurate way to measure quickly changing, sensitive temperature variations. Thermocouples are able to read a wide range of temperatures accurately and reliably, but they must be monitored over time due to degradation from corrosion and other effects of overextending a thermocouple's use [7]. Figure 8 shows the type of thermocouple used on the TCR. The thermocouple probes are used to measure the stagnation velocity by being housed in a cavity that, like the stagnation pressure probes brings the flow isentropically to rest. This is discussed in more detail later.

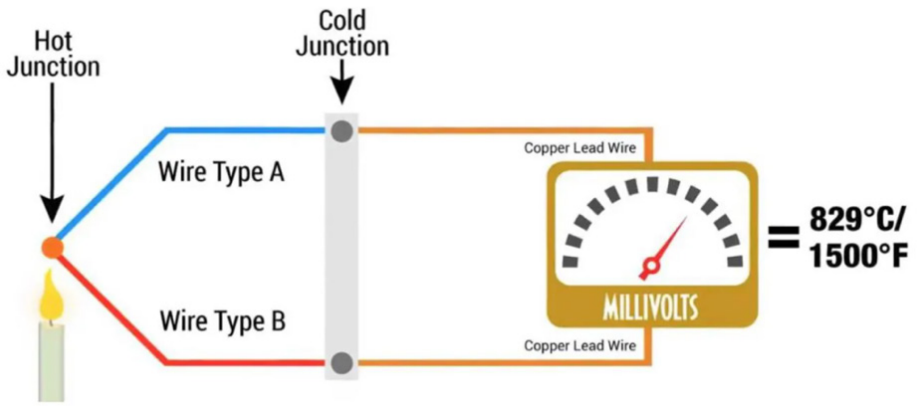


Figure 7. Diagram of how thermocouples work. Source: [8].

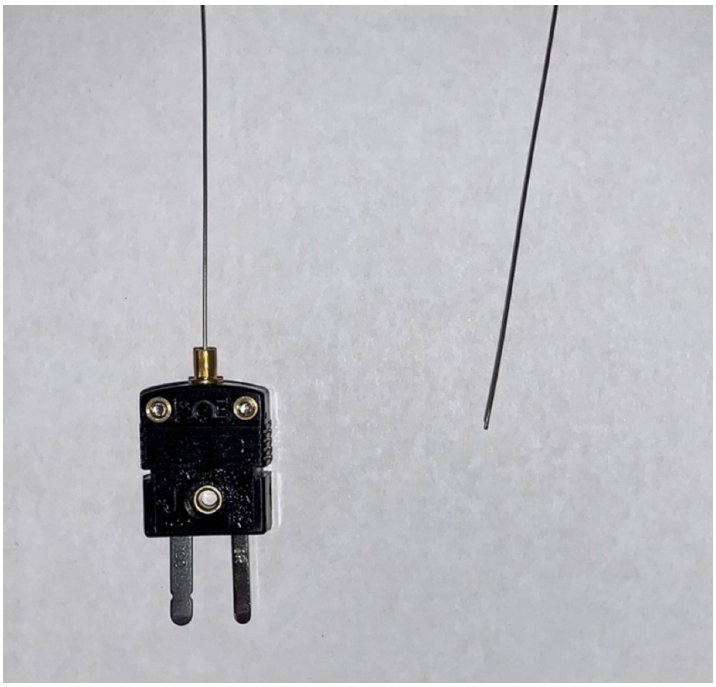

Figure 8. Close view of the mini plug and end junction for the thermocouple used on the TCR.

Although not in current use on the TCR, two more forms of velocity instrumentation that could be introduced if there was more design freedom are hot-wire anemometers and LDVs. Hot-wire anemometers have been researched at the TPL in the past but cannot currently be used in the downstream casing [9]. A hot-wire anemometer works by first heating a tungsten, platinum, or platinum-iridium wire by running an electric current through it. Next, as fluid moves around the wire, the velocity of the flow may be correlated to the velocity through the measured heat rejection through convection. Hot-wire anemometers are an accurate way to measure the velocity of the flow while introducing minimal blockage [9]. Another benefit of hot-wire anemometers is that they are highly sensitive to changes in velocity. Figure 9 shows a diagram of the parts of a hot-wire anemometer. One problem with hot-wire anemometry is that the devices are sensitive and often require replacing. The current casing makes this difficult.

The other form of velocity instrumentation that could be introduced to the TCR that is not currently implemented is an LDV. LDVs similarly measure the instantaneous velocity of the flow with a high frequency response by measuring the reflected radiation of

a particle in the flow from a laser beam sent into the flow, as the diagram in Figure 10 portrays. The velocity of the flow is calculated by utilizing an induced Doppler effect. The greatest benefit to the LDV is the non-intrusive nature of the measurement. The downsides of the LDV include a necessity for a transparent window into the flow to send a laser beam, reduced accuracy, and increased cost [10].

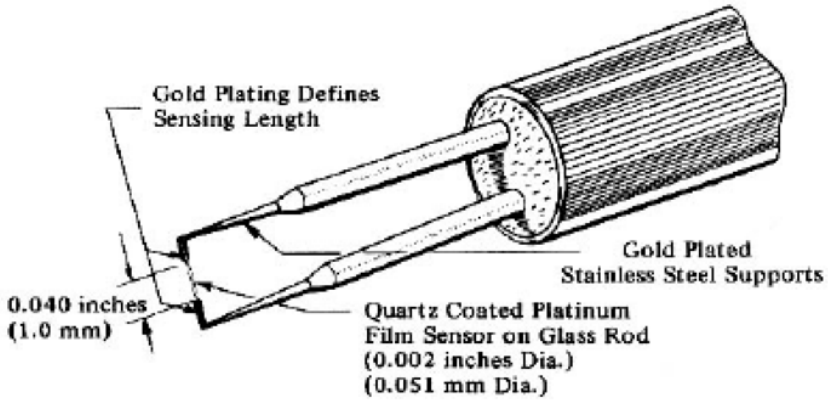


Figure 9. Diagram showing the parts of a hot-wire anemometer. Source: [11].

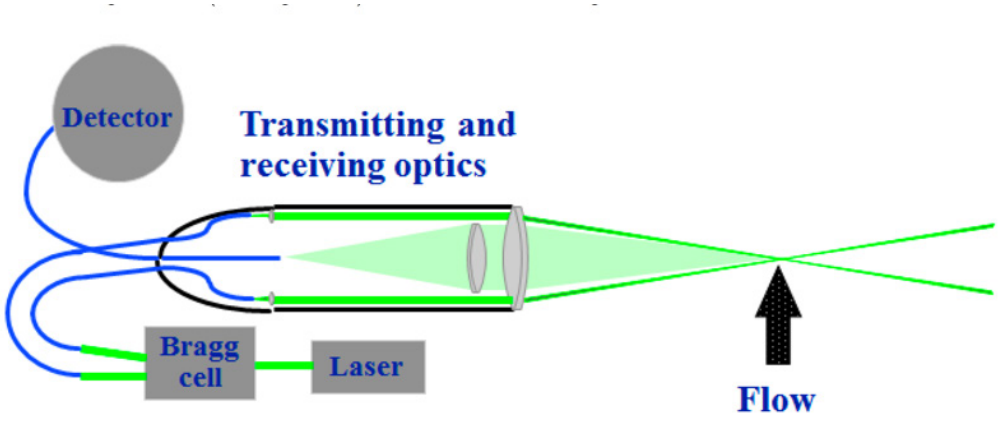


Figure 10. Diagram of how LDVs measure a flow field's velocity. Source: [12].

## 2. Discussion of the Credibility of CFD Software

Computational fluid dynamics (CFD) software is one of the most widely used tools in the field of fluid mechanics. Its primary function is to calculate the pressure, temperature, and flow of a particular fluid scenario using the Navier-Stokes equations. These equations act as governing equations, ensuring the conservation of physical properties of the fluid. Prior to the advent of high-speed digital computers, the manual calculation of the Navier-Stokes equations was an incredibly tedious and repetitive process. However, computers have made it possible to solve fluid dynamics problems with incredible accuracy by using these equations. In the past, the only way to solve such problems was through experimentation and theoretical calculation. With CFD, it is possible to obtain accurate solutions from the Navier-Stokes equations without having to make overly simplifying assumptions. The advantages of CFD are numerous, including a significant reduction in the cost of experimentation. CFD can generate the results of hypothetical experiments using only a computer in a fraction of the time it would have taken to run the physical experiment. Numerical analyses comparing the accuracy of CFD to experimental results have consistently shown that modern simulations provide more than reasonable solutions to fluid dynamics problems. As a result, CFD has become a commonly used tool in research in general and hence was used in this thesis to guide the design of the downstream rake probes [13].

## 3. Common Practices, Benefits, and Constraints of Additive Manufacturing

Additive manufacturing (AM), or 3-D printing, has become dramatically more prevalent in recent years for all the substantive benefits the technology provides. There are different types of 3-D printing including powder bed systems, extrusion based systems, and sheet lamination processes [14]. A few areas of consideration when choosing which type of technology would be best include cost, geometry, and building material. Regardless of which type of 3-D printing would be the most appropriate, AM can provide shorter lead times, more design freedom, and increased savings. AM removes the supply chain as a factor when performed in-house. Additive manufacturing is also beneficial over subtractive manufacturing, or machining, in that less material is used. Potentially the largest benefit

comes from the increased design freedom. No longer do engineers have to choose from a list of machining constraints that may not be the optimal solution. Instead, AM offers engineers an ability to create an innovative solution. All they have to do is use CAD software to draft the solution within the bounds of the printer's capabilities and send it to the printer.

### 4. Capabilities and Limitations of the EOS M 100

Shown in Figure 11 is the same EOS M 100 3D printer that is housed at NPS. Although several 3D printers could have been used for this research, the EOS M 100 was the readily available printer and was the focus of this research. The EOS M 100 is a metal printer created by EOS that utilizes powder bed fusion to build its parts. The printer works by uploading an .stl file to its EOSPRINT software. An STL file approximates a solid by unstructured triangulated faces. STL stands for stereolithography. Its other software, known as Magics, is then used to apply support structures to the build and specify the printing conditions of the part. Once this is complete, the job can be sent to the printer. The print is then completed in an argon filled container by spreading a fine layer of metal powder and melting it with a laser in the exact specified location of interest. This process is repeated until the build is complete [15]. The maximum build size is approximately 10 cm x 10 cm x 9.5 cm (3.94 in x 3.94 in x 3.74 in) with a minimum layer thickness of 0.1016 mm (0.004 in) [16]. Another constraint found from past work was that the maximum cantilever angle that the NPS EOS printer could still print accurately was approximately 45°. All of these constraints had to be taken into account when coming up with a potential instrumentation solution.


Figure 11. The same EOS M 100 model used at NPS. Source: [17].

## C. OBJECTIVES AND THESIS OVERVIEW

With these concepts in mind, the first objective was to design a casing that would fit within the design requirements to establish a baseline for which the instrumentation could be improved upon. How this objective was completed can be found in Chapter II. The second objective, which can be found in Chapter III, was to design a baseline insert that would interface with the casing from which pressure and temperature probes would be designed to measure from. Following this objective, a CFD analysis was conducted on the stator to better understand which measurement locations would be most effective. This CFD analysis can be found in Chapter IV. The last objective was to tie all of this together by designing pressure and temperature instrumentation inserts to be printed to effectively measure and report the internal characteristics of the TCR in locations found to be most critical from the CFD analysis that was completed. The process to design these pressure and temperature probes can be found in Chapter V. Lastly, all plans for future work can be found in the conclusion in Chapter VI.

# II. INSTRUMENTATION CASING DESIGN

The first step in creating a more accurate and repeatable way to measure the pressure and temperature within the transonic compressor was to establish a datum from which to measure. As stated earlier, the old design led to numerous configurations and lacked redundancy and repeatability. The entire instrumentation casing was to be redesigned to have flat sections to which instrumentation inserts could be easily and repeatably secured. Additionally, the instrumentation casing was to be redesigned to allow for additively manufactured instrumentation inserts that would increase the number of total measurements on the rig.

## A. CASING DATUM CONSTRUCTION

The original design intent took inspiration from the upstream IGV casing which was similarly constructed to have flat sections machined out of the overall cylindrical casing. One of the main differences between the IGV casing and the to-be-designed instrumentation casing was that the instrumentation casing would not have the constraint of having a cylindrical exterior which is imposed by machining on a lathe; the entire exterior of the instrumentation casing would be configured with flat sections. This makes the positioning and changing of probes simpler and more accurate. With this, the first step was to identify a polygonal shaped casing perimeter that would maximize future design freedom while maintaining structure requirements and keeping a consistent interface with upstream and downstream components. Figures 12–14 display how the polygonal structure was identified.

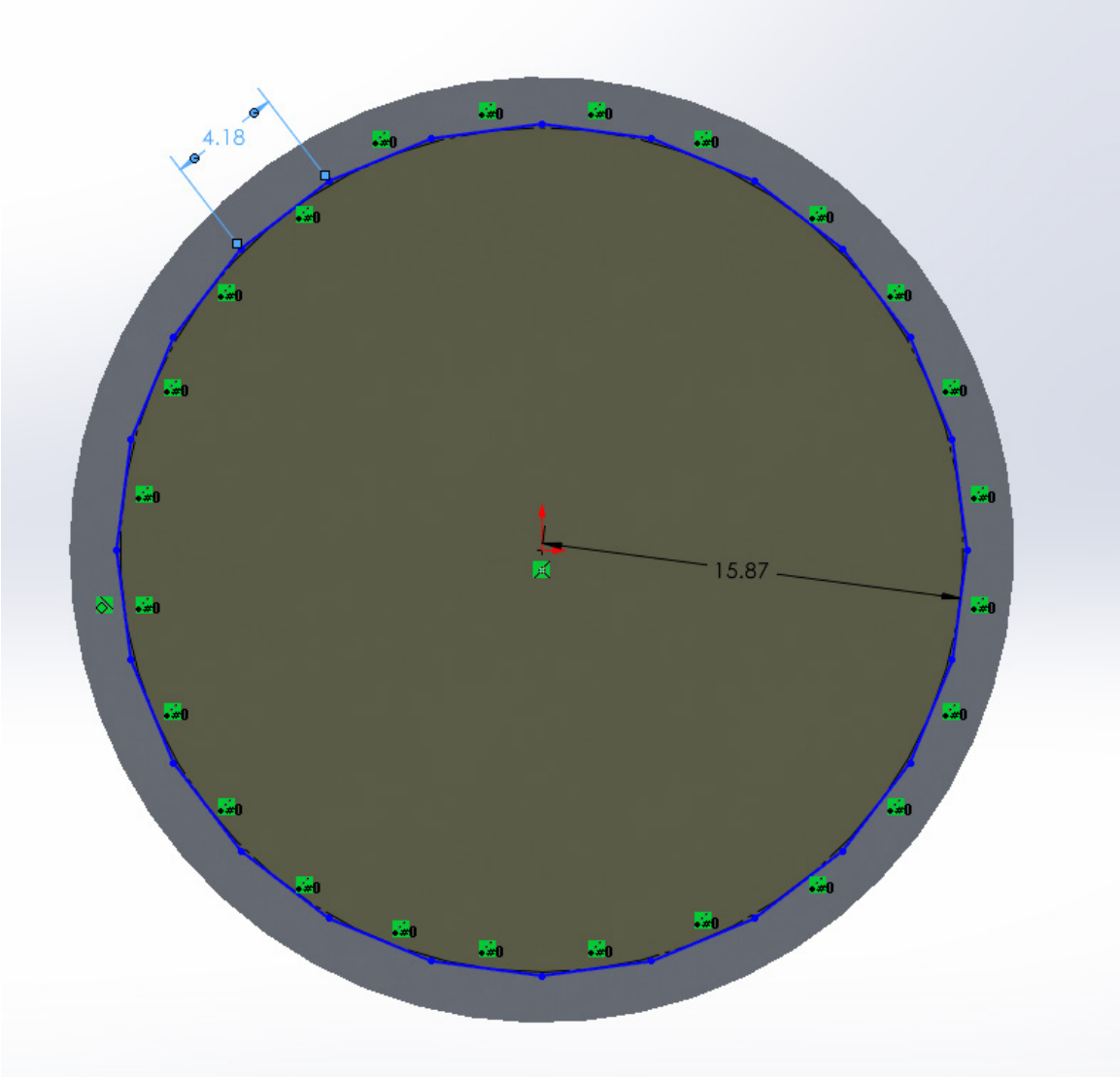


Figure 12. Example polygonal structure for 24 even sides (dimensions in cm).

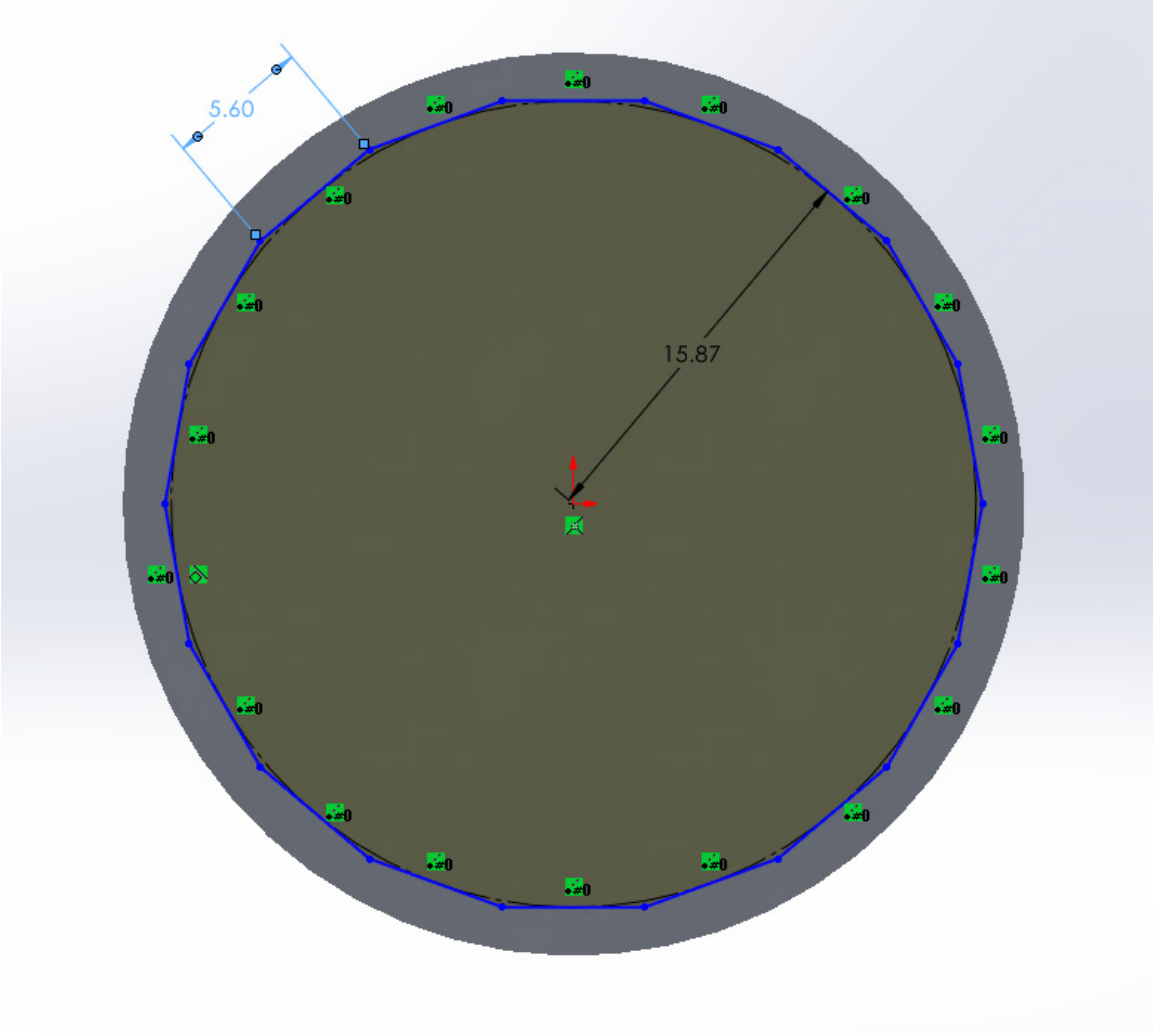


Figure 13. Example polygonal structure for 18 even sides (dimensions in cm).

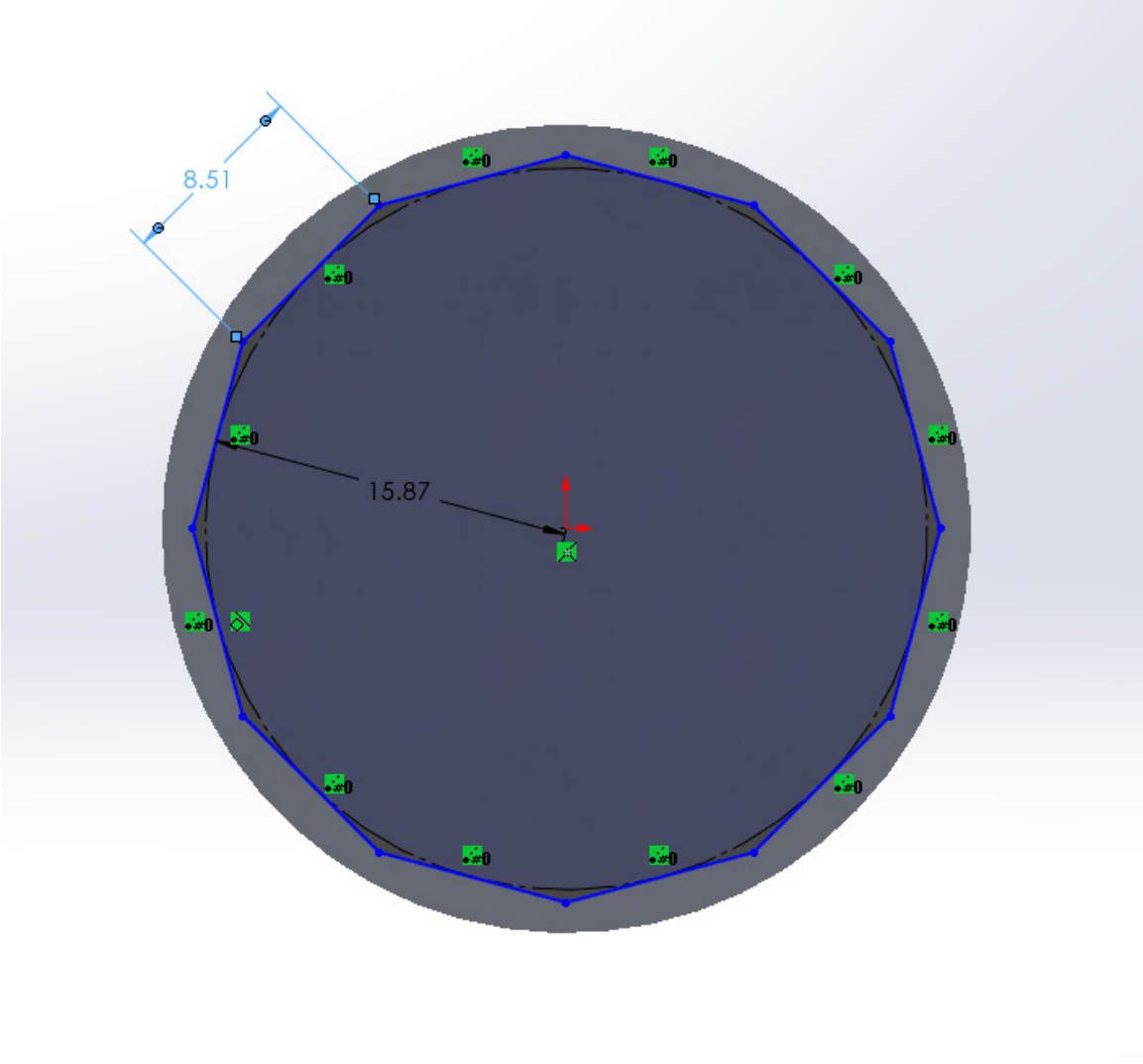


Figure 14. Example polygonal structure for 12 even sides (dimensions in cm).

At the outset of the present work a few key design decisions were made. These decisions centered around the number and size of sides the polygonal structure would have. The design requirements ultimately limited the number of design configurations. Table 1 shows the list of design requirements for the instrumentation casing.

Table 1. Requirements analysis of the instrumentation casing design.

| |
|---|
| 1. Casing shall maintain the same interface with upstream and downstream components<br>a. To include: front to back length, location of upstream and downstream bolts, and conforming geometry for mating parts |
| 2. Casing shall have distinctly different sized sides that allow for future design freedom to incorporate other instrumentation |
| 3. Number of casing sides shall be a multiple of six to match bolt periodicity |
| 4. The perpendicular going through the midpoint of each casing side shall be in line with center of the rig |
| 5. Casing shall be able to be produced by a machinist |
| 6. Casing shall maintain at least the same thickness as the old casing within 0.254 cm (0.10 in) |

The first design requirement for the casing was that the upstream and downstream interfaces between casings had to be the same. It was impractical to alter the other components on the rig to accommodate the instrumentation casing. As such, it was determined that the number of sides of the polygonal shape had to be a multiple of six. This was due to the six bolts on the forward flange that secured the instrumentation casing to the upstream casing. The first design decision to be made was the number of sides to the polygon. By having the number of sides be 12, 18, or 24, there would be a repeating pattern between the sides and any interference with the bolt, such as in Figures 12–14. Intuitively, the number of sides had a direct impact on the size of the sides; more sides meant the size of each side would have to be smaller. Any number of sides less than 12 or greater than 24 led to the sides being too large and too small, respectively. The second main decision was how to size each side. The most interference between the sides and the bolts appeared where two sides formed an angle as this was point was the greatest distance from the center of the rig. These considerations quickly narrowed the search down to the four options presented in Table. 2.

Table 2. Comparison of potential casing side sizes (side depth x side length).

| 12 Equilateral | 18 Two-Sized | 18 Equilateral | 24 Equilateral |
|---|---|---|---|
| 3.988 cm x 8.509 cm (1.57 in x 3.35 in) | 3.988 cm x 4.216 cm/3.988 cm x 8.382 cm (1.57 in x 1.66 in/ 1.57 in x 3.30 in) | 3.988 cm x 5.588 cm (1.57 in x 2.2 in) | 3.988 cm x 4.191 cm (1.57 in x 1.65 in) |

Another design requirement maintained that a perpendicular line on each side starting at the side's midpoint would pass through the center of the rig which would ensure that any temperature and pressure probes designed to penetrate the rig at the midpoint of each side would radially point exactly at the center. If there were to be two different sized sides, as also specified in the requirements, this requirement essentially forced there to be 18 sides.

Lastly, the design was required to be structurally sound and machinable. The initial design requirement for material thickness of the casing mandated no thickness less than that of the current instrumentation casing. This requirement created significant design challenges and was later relaxed to meet the intent of maintaining structural stiffness and strength. Eventually, the requirement was accomplished by ensuring the design would be no more than 0.254 cm (0.10 in) thinner at any point on the new design compared to the old design. In the end, the polygon that was chosen was designed by creating a 24-sided polygon centered around the center axis of the rig which was altered into an 18-sided polygon by combining the third and fourth sides into one large side in a pattern that repeated every four sides around the rig. Next, this shape was scaled to a machinable size that was less than 0.254 cm (0.10 in) thinner than the old design. An image of this solid is shown in Figure 15.

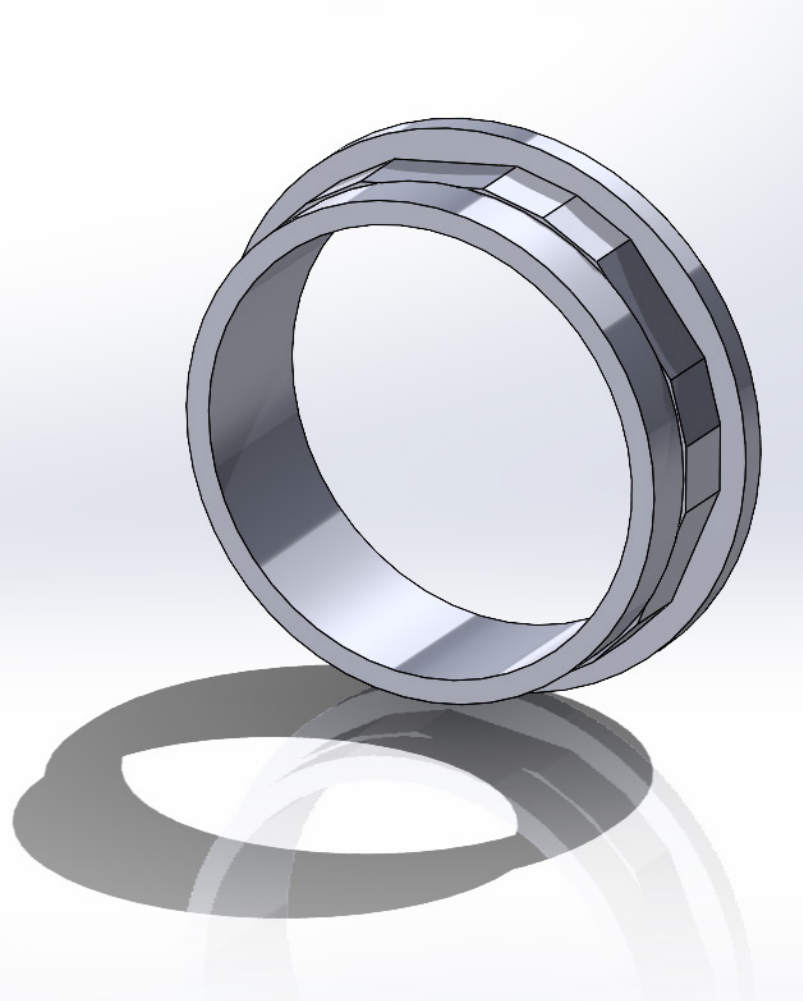

Figure 15. Designed casing with flat sections specified but no inserts.

Once the shape of the flat sections was determined, the final, undetermined dimension of the sides was axial length. The old design was simply cylindrical from the flange to the back. Because the flat sections would not match the downstream mating component, an axial extrusion length had to be determined. The former design interface was measured, analyzed, and it was determined that an extrusion length of 4.318 cm (1.70 in) was the most optimal as it maximized the usable surface for the instrumentation while allowing an axial translational tolerance of 0.318 cm (0.125 in). The size of each flat section was known at this point, as seen in Figure 16, which meant the size of each insert could be determined next.

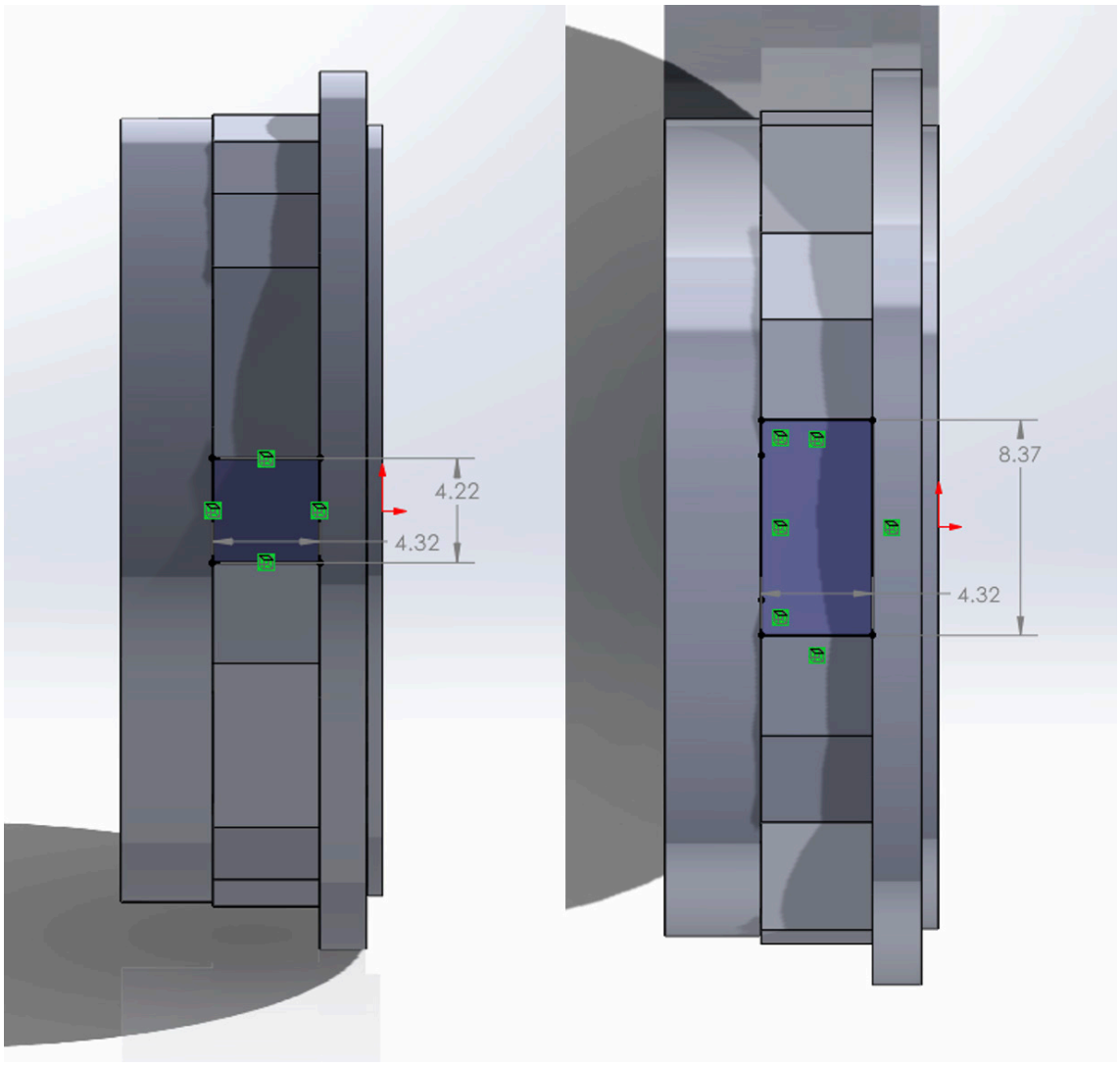


Figure 16. Size dimensions of the two different sides (dimensions in cm).

## B. INSERT SIZING DIMENSIONING

With the sizes of each flat area known, the size of the inserts could then be determined. Many of the requirements identified in Table 1 still applied. The goal of the insert dimensioning was to maximize the insert space, and thus future design freedom, while ensuring structural integrity and machinability. There were several configurations that could have been chosen, but in the end after consulting with the NPS resident machinist, it was decided that a rectangular cut with rounded corners specified to a common drill bit's size and dimensions from the edges of the flat section would be the best from a

machinability perspective. This configuration offered the optimal balance between coast and the specified precision required. With this, all inserts were specified to have 0.318 cm (0.125 in) radius curves at the corners. The insert cutouts were also to be 1.27 cm (0.50 in) from the seam between flat sections. Additionally, the cutouts were to be 0.508 cm (0.20 in) from both the forward flange and transition point between flat section and cylindrical exterior to the back. These dimensions would ensure structural integrity while providing ample space for bolts to be designed to screw the inserts into the datum surface.

## C. HOLE SIZINGS AND LOCATIONS

At this stage in the design process, the amount of usable flat area was known so the desired bolts to secure the instrumentation plugs could be chosen based on size. Again, machinability was a factor. To simplify the design from a machinability perspective, the bolt holes were designed to be smoothly machined to allow for screw inserts to be placed into each bolt hole. The other primary factor, similar to when deciding on the insert dimensions, was deciding the minimum allowable thickness between the holes and the ends of the casing. Balancing these two factors, a COTS (commercial off the shelf) stainless steel key-locking helical insert was found to match an ultra-low profile 5/16” 10–32 socket head screw. If the bolt hole was placed 0.650 cm (0.256 in) from each edge of the flat area, the minimum thickness would be 0.318 cm (0.125 in) between the bolt hole and the insert cutout. The locations of all other holes on the casing, such as those on the front flange and downstream cylindrical portion, were kept the exact same as on the old design. This ensured that the interface between casings would be kept the same.

## D. COUNTERBORE IMPLEMENTATION

When considering initial design of the instrumentation inserts, it was quickly apparent that the interference with the bolts on the forward flange would have to be addressed. Because of this, a counterbore on the front flange around the bolts was included. The counterbore depth was made to be the same depth as the protrusion of the screw with the washer. This way the bolt would not extend downstream over the instrumentation flat sections beyond the front flange. Again, there were a few ways that this result could be achieved from a machining perspective. After the NPS machinist was consulted, it was

found that the most effective way to accomplish this was to cut into the flange using a 1.270 cm (0.50 in) radius drill bit tangential to the flat then cut outward radially. This allowed a wrench to fit around the bolt and rotate more than 60° to make maintainability more efficient and simpler. This counterbore was included on all six bolts on the front flange, but not the three holes used during disassembly.

Lastly, all chamfers and fillets present on the old casing were designed for the new instrumentation casing. At this point the entire casing was designed exactly to the specifications that would best benefit the TPL. Figures 17–19 show different angles of the final instrumentation casing design. The engineering drawings of the final instrumentation casing can be seen in Appendix A.

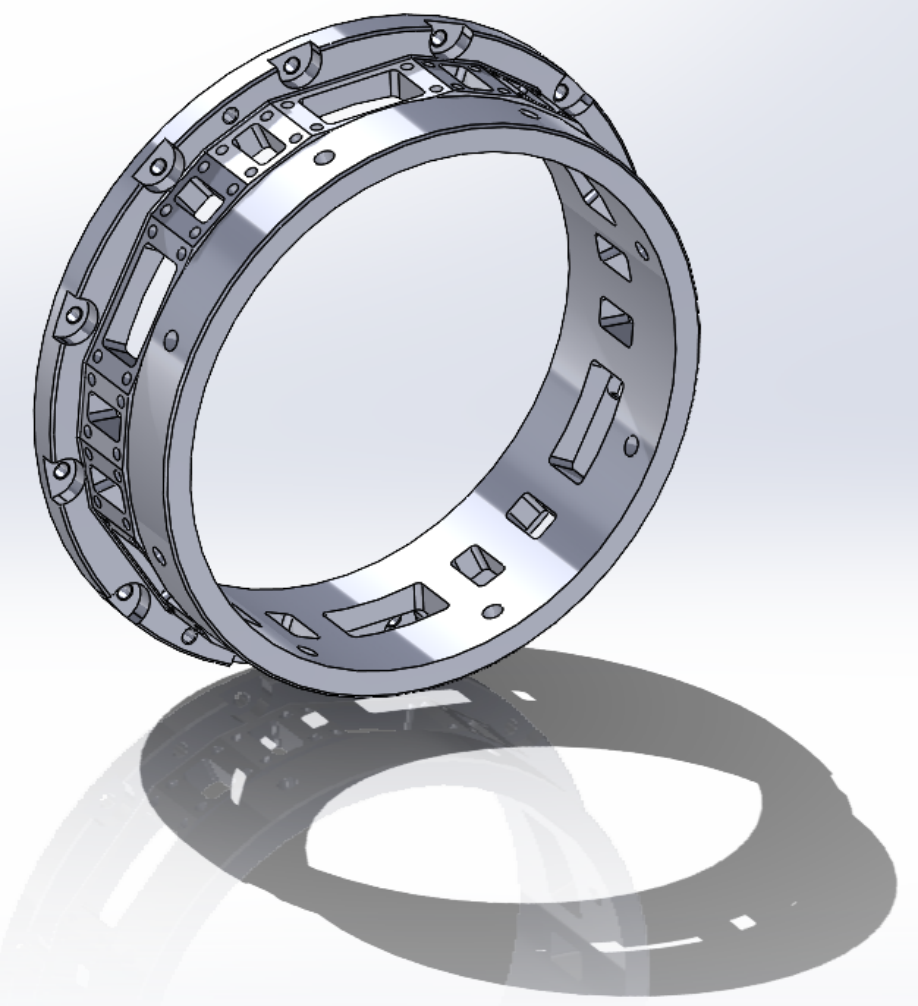

Figure 17. Side view of the final instrumentation casing from the downstream angle.

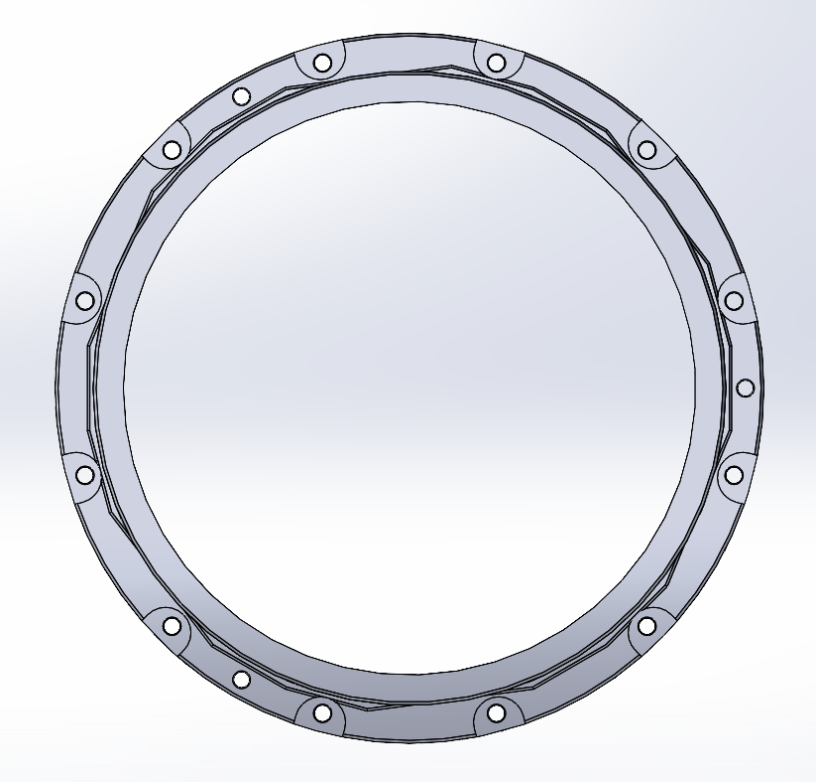

Figure 18. Axial view of the final instrumentation casing from downstream.

Figure 19. Side view of the final instrumentation from upstream.

# III. DATUM UNIVERSAL MEASUREMENT INSERT (DUMI)

After the instrumentation casing design was complete, the interface between the casing and the instrumentation inserts could be designed next. This was done by first designing a baseline insert that would seal the casing. This baseline insert would also be the baseline from which pressure and temperature probes would be designed. This baseline insert became known as a datum universal measurement insert. Because there were two different sized datum sections, two different sized DUMIs were designed but both utilized the same design process as is described in the following sections.

## A. DESIGN REQUIREMENTS

At this stage, the DUMI design was guided by numerous requirements. The requirements analysis for the DUMI can be seen in Table 3. The two most imperative requirements for the design were that the DUMI had to adhere to the same interface as designed into the casing and the insert could not interfere with the casing's bolts on the front flange.

Table 3. List of DUMI design requirements.

| |
|---|
| 1. DUMI shall match the sizing and interface provided by the datum surface of the designed instrument casing |
| 2. There shall be two DUMI designs (one large and one small) |
| 3. DUMI shall be designed to allow the upstream casing to be disassembled without necessitating the removing the inserts |
| 4. DUMI shall fit within the print limitations of the EOS M 100 |
| 5. DUMI shall be a structurally sound system without any forces designed to be applied that may deform the structure of the DUMI |
| 6. DUMI shall provide a seal with the rig which allows no air flow to pass through the casing sides |
| 7. Internal surface of the DUMI shall have the same radius as the internal wall of the casing |

## B. DESIGN PROCESS AND CASING INTERFACE

First off, requirement one stated that the DUMI was required to fill the gaps in the casing meant for the insert. This rectangular shape had to be extruded from the datum surface radially toward the center of the rig. To not interfere with the flow through the rig, the most internal surface of the DUMI was designed to match the internal wall radius of the rig, requirement seven.

The following step was to design the surface that would secure the DUMI to the casing. The locations for where the helical inserts, and their corresponding screws, would be placed were known. Therefore, the first step in the design of this surface was to create through holes for the screws to secure the DUMI to the casing. The next question was how thick this surface could be. To ensure that the casing would be able to be unscrewed without taking out all the instrumentation, this portion of the DUMI was made to be 0.102 cm (0.040 in) thick so a wrench could fit around the screw on the front flange to unscrew the bolt even with the DUMIs secured to the casing.

The last design requirement to meet was to provide a clean, airtight seal between the DUMI and the casing. Flat gaskets, grease, and room temperature vulcanizing silicones were some devices that could have been used to seal the casing, but ultimately an O-ring was decided to be the optimal design. There were multiple orientations for O-rings that could be used, but two specifically appeared to be most beneficial. One idea was to place the O-ring on the bottom side of the DUMI to be squeezed between the DUMI and the external surface of the casing. The other idea was to design an O-ring groove into the portion of the DUMI that would slide into the casing. In the end, it was decided that the latter would be a more effective design as this orientation allows the casing sides to be used as they are intended as well as implement a hermetically sealing design that is also self-centering within the slot. If the O-ring were to be compressed between the external surface of the casing and the DUMI, when the DUMI would be screwed into the casing, the location of the measurements would be dependent on how compressed the O-ring was. There was no specific need to have a particular O-ring cross section, thus a readily available standard O-ring cord size of 0.178 cm (0.070 in) diameter O-ring material was used as the groove sizing standard. Second, a resource was found from Global O-ring and Seal which specified

the sizing of the groove required to provide a clean seal for an O-ring. The type of O-ring seal decided upon is a static gland seal. This orientation is used to seal two nominally stationary mated surfaces that must have a designed gap to allow assembly. A standard readily available design guide was used to specify dimensions for this seal type and O-ring size. The parameters and graphic for this are shown in Figure 20. As seen in the top row for 0.178 cm (0.070 in) diameter O-rings, the groove had to have a depth of 0.132 cm (0.052 in) and width of 0.241 cm (0.095 in). This groove was implemented in the DUMI design at the midpoint of the section that slides into the casing. A fillet is at the internal corners of the groove as well as the edge leading into the groove with a radius of 0.127 mm (0.005 in) to abide by the specifications provided. [18]

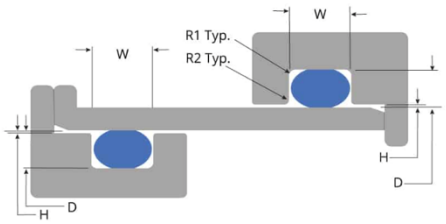


| AS568 Series | O-Ring Cross-Section | | Gland Depth (D) | Squeeze | | Gland Width (W) | | | | Gap (H) | Gland Corner Radii | |
|---|---|---|---|---|---|---|---|---|---|---|---|---|
| | Nominal | TOL (+/-) | | Actual | Percent | Nominal | TOL (+/-) | w/ 1 Backup Ring | w/ 2 Backup Rings | MAX | R1 | R2 |
| -0XX | 0.070 | 0.003 | .050-0.052 | .015-.023 | 22%-32% | 0.095 | 0.002 | 0.140 | 0.207 | 0.002 | 0.007 | 0.005 |
| -1XX | 0.103 | 0.004 | .081-.083 | .017-.025 | 17%-24% | 0.142 | 0.003 | 0.173 | 0.240 | 0.002 | 0.007 | 0.005 |
| -2XX | 0.139 | 0.004 | .111-.113 | .022-.032 | 16%-23% | 0.189 | 0.003 | 0.210 | 0.277 | 0.002 | 0.017 | 0.005 |
| -3XX | 0.210 | 0.005 | .170-.173 | .032-.045 | 15%-21% | 0.283 | 0.003 | 0.313 | 0.412 | 0.003 | 0.027 | 0.005 |
| -4XX | 0.275 | 0.006 | .226-.229 | .040-.055 | 15%-20% | 0.377 | 0.003 | 0.410 | 0.540 | 0.003 | 0.027 | 0.005 |

Figure 20. O-ring sizing guidance provided by Global O-ring and Seal. Source: [18]

The baseline insert that would seal the flow was known at this point. For any flat section that did not need instrumentation, a DUMI would satisfy the need to plug the hole in the casing. Figure 21 displays the final design of the DUMI from which pressure and temperature instrumentation could be designed.

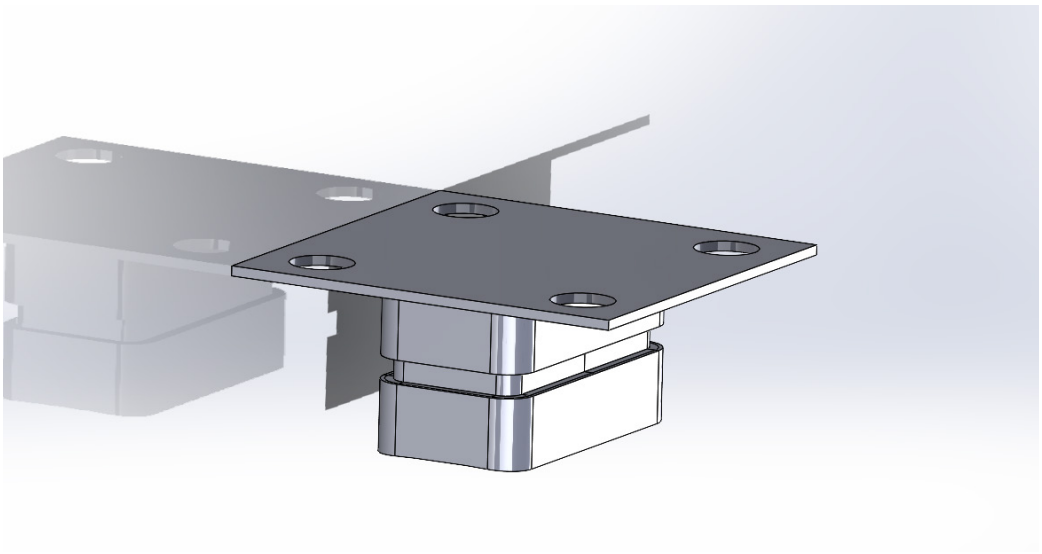

Figure 21. Final design of the small flat section DUMI.

# IV. STATOR CFD ANALYSIS

Designing more effective pressure and temperature probe systems to measure the internal flow characteristics of the rig accurately and effectively was the next step in optimizing the instrumentation on the TCR. This optimization cannot be done without some a priori information about the nature of the flow field as any number of modifications to the compressor stage under test can alter flow field characteristics. To estimate the characteristics of the flow field aft of the compressor stage, a CFD analysis was completed on the stator to simulate what the characteristics of the flow were through the stator and past the instrumentation casing. This constituted the first meaningful computational analysis using CFD on the stator component of the NPSMF as most of the focus has been on the rotor. The purpose of the analysis was to better understand the nature of the pressure and temperature fields behind the stage at the instrumentation location. The outline that follows is consistent with the ANSYS-CFX outline used to complete the CFD analysis. Computational analyses begin with geometry construction followed by mesh generation, computational setup, and results analysis of the CFD experiment.

## A. DOMAIN CONSTRUCTION

The geometry of the gas path was created to be $1/29^{th}$ of the circumference of the rig around the cavity of one stator blade. Axially, the gas path was created to extend from the front of the stator back past the location of the rake probes to be designed later. This setup can be seen in Figure 22. The arrows show the flow of air through the rig. The white rectangle shows the location of the future pressure or temperature measurements. A cavity of the stator was taken to cut out the stator blade within the domain and shape the top and bottom walls of the domain.

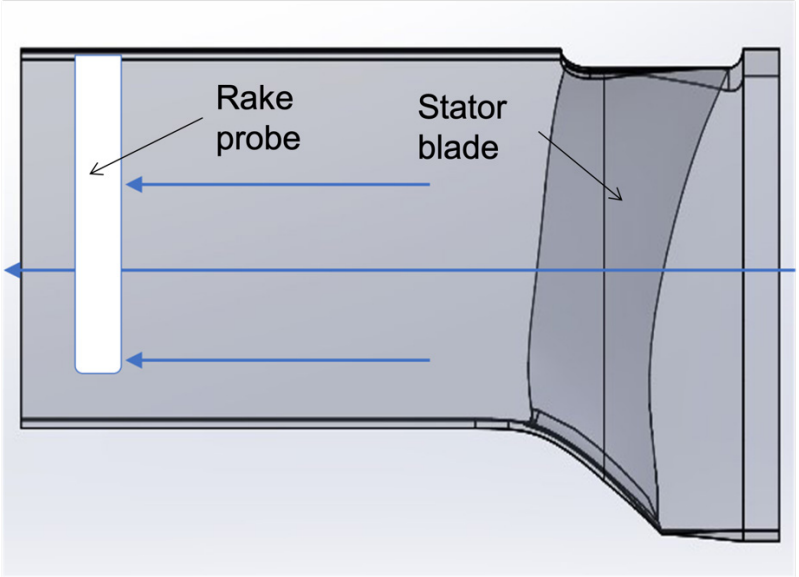


Figure 22. Gas path around the stator blade.

## B. MESHING GENERATION

A mesh of the geometry was completed that resulted in 2,266,436 elements with 1,067,241 nodes. This mesh included an inflation layer with first layer height of 5e-7 m (or 0.5 μm) with a maximum of 40 layers and growth rate of 1.2. Additionally, as mentioned earlier, the geometry was 1/29$^{th}$ of the entire rig, so the mesh of each side of the geometry had to match with each other to increase the computational efficiency and accuracy by minimizing any interpolation errors between sides. As such, the match control feature in CFX ensured that this would be true. An image of the mesh can be seen in Figure 23.

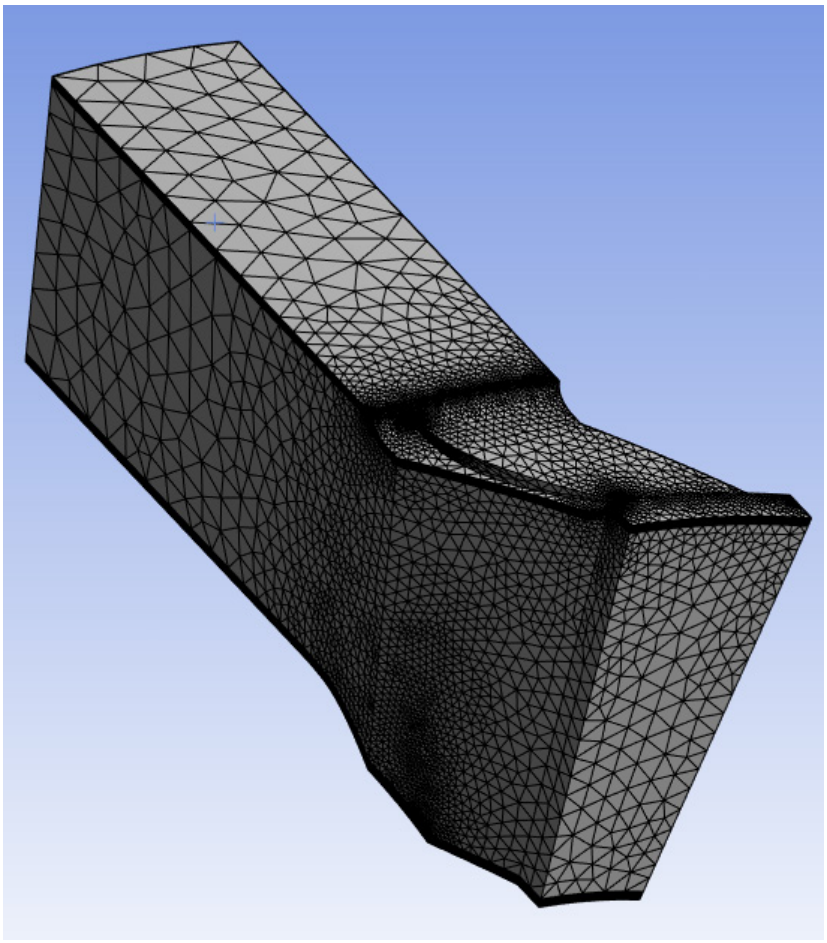

Figure 23. View of the gas path's mesh.

## C. CFD SETUP WITH ROTOR OUTPUT IMPLEMENTED

With the mesh complete, the next step was to outline the experimental setup. Cyclic sides were specified for each side of the domain to again ensure the constant values for the periodicicty of the domain. Next, the downstream face was specified to be an outlet and the top, bottom, and blade cutout faces of the domain were specified to be a no slip wall. The last step was to specify the conditions of the inlet. Because the flow into the stator from the rotor was rotating and moving axially, a theta and axial velocity was specified at the inlet. Figures 24 and 25 show where these conditions were derived from. An average for 90% performance at peak efficiency was taken across the radius for both rotational and axial velocities [19]. From this, 100 m/s was specified for the axial velocity and -75 m/s was specified for the rotational velocity. The average total pressure and total temperature

at the inlet were also specified from similar data. For this analysis, a Shear Stress Transport (SST) turbulence model, total energy, and ideal gas setup was used to compute the highest fidelity model.

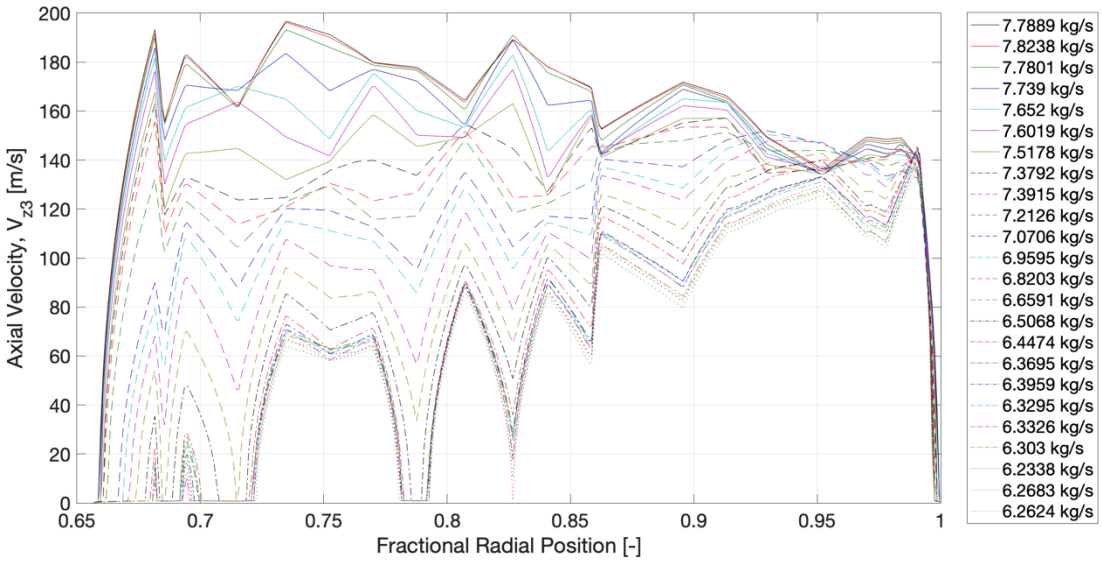


Figure 24. Experimentally measured axial velocities at 90% performance across the radius.

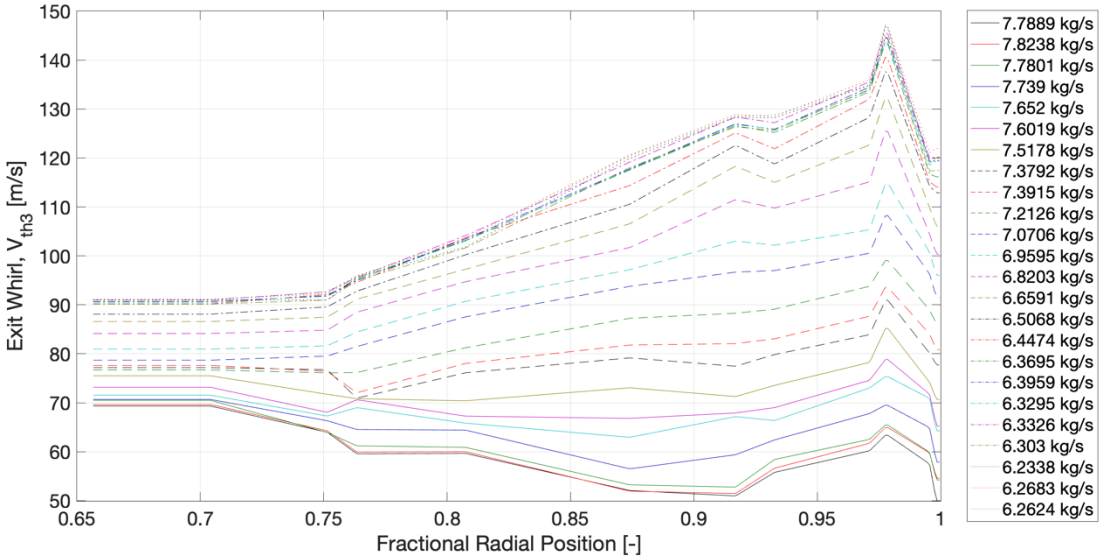


Figure 25. Experimentally measured angular velocities at 90% performance across the radius.

## D. CFX RESULTS ANALYSIS

After the experiment was completed, the next step was to confirm that what was found was indeed reliable. The first step was to analyze the residuals. As it turned out, the residuals converged enough for the purposes of the endeavor with values less than 1e-3, as seen in Figure 26. As this is a design calculation to gain insight into the flow field pressure and temperature distribution, it was determined that the residuals passed the residual convergence test.

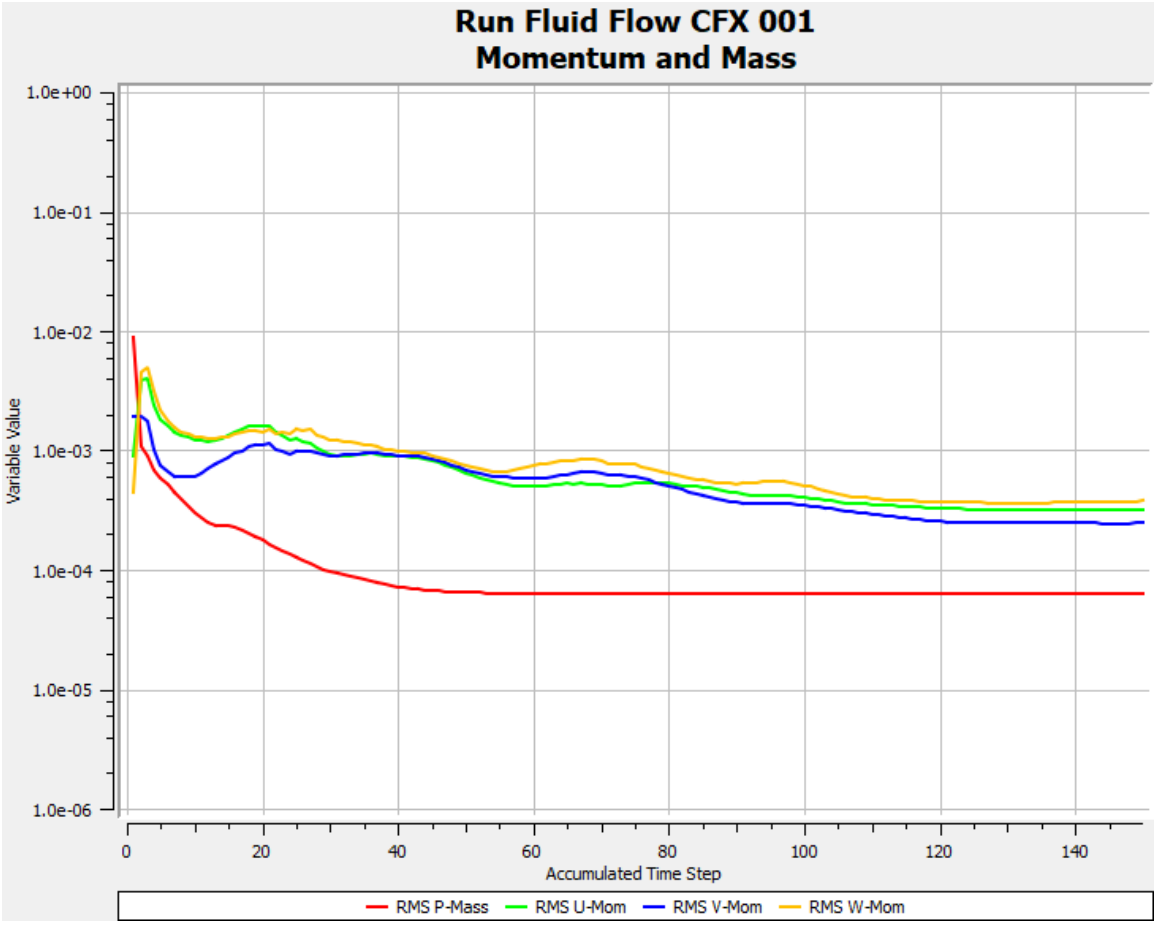


Figure 26. Plot of the residuals.

After the residuals analysis, the $y^+$ value on the wall was measured and evaluated as seen in Figure 27. The results of the analysis showed that the $y^+$ value at the wall, as given by

$$y^+ = \frac{u^* y}{v} \quad (1)$$

where $u^*$ is the friction velocity, y is the distance from the wall, and v is the kinematic velocity, are evaluated at one or below. A criterion for wall resolution of the SST turbulence model is a $y^+$ value less than ten and close to one. Having met the criteria, the near wall mesh resolution was judged to be appropriate for the model. A complete CFD report for this experiment can be found in Appendix B.

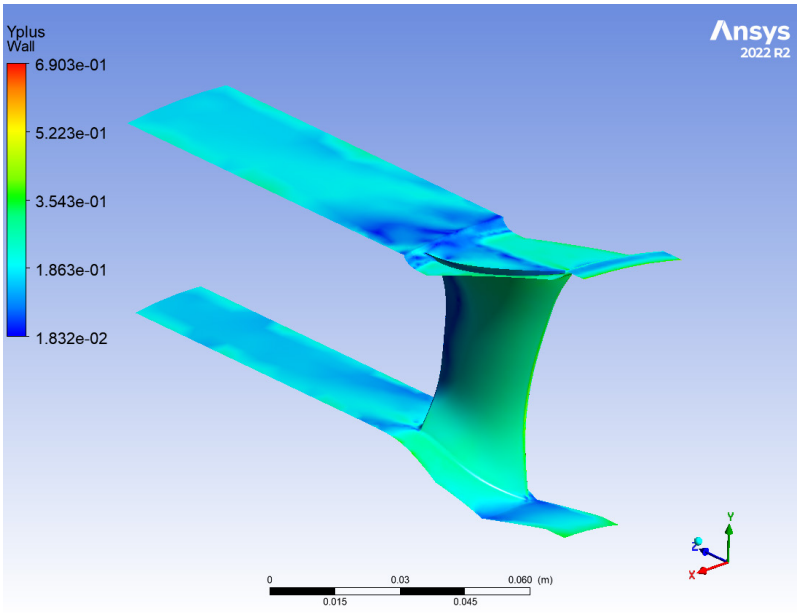


Figure 27. Map of $y^+$ on the wall.

Once the residuals and $y^+$ values were confirmed, the useful information from the model for which the project was created could be extracted. Figure 28 shows where measurement of the total temperature along the plane where the temperature probes will take their measurements could be placed. Similarly, Figure 29 shows the measurements for total pressure, where different probes could take pressure measurements. On the top side of each figure, a grey rectangular shape shows potential locations of these measurements on figurative probes. The purpose of these probe measurements was to be located in such a way that would accurately display the graphs in the middle of the figures with the fewest number of measurements required. The next step was to determine the most efficient way

to do this combining unique and redundant measurements across the different pressure and temperature probes located around the rig.

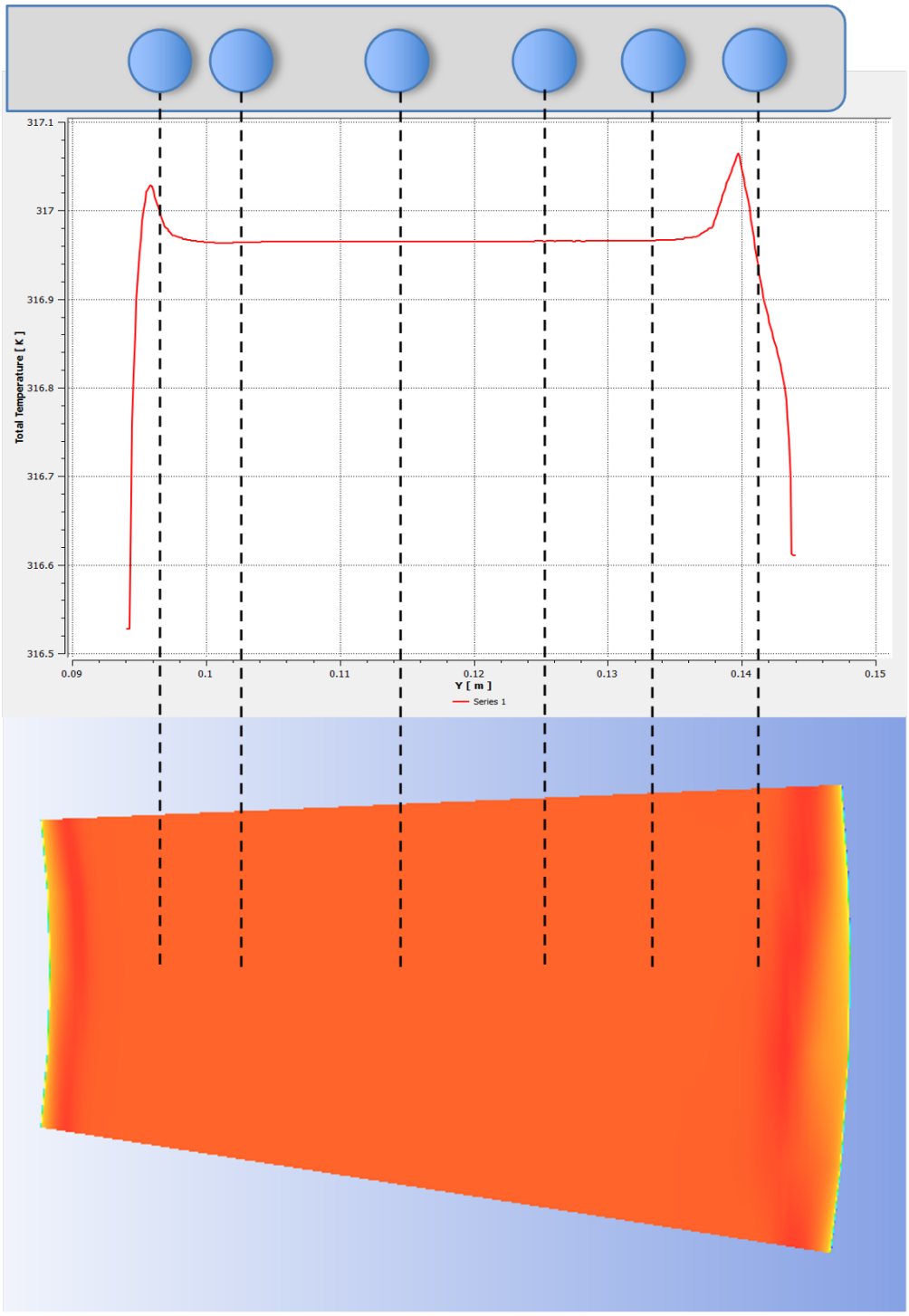


Figure 28. Plane measurements for total temperature.

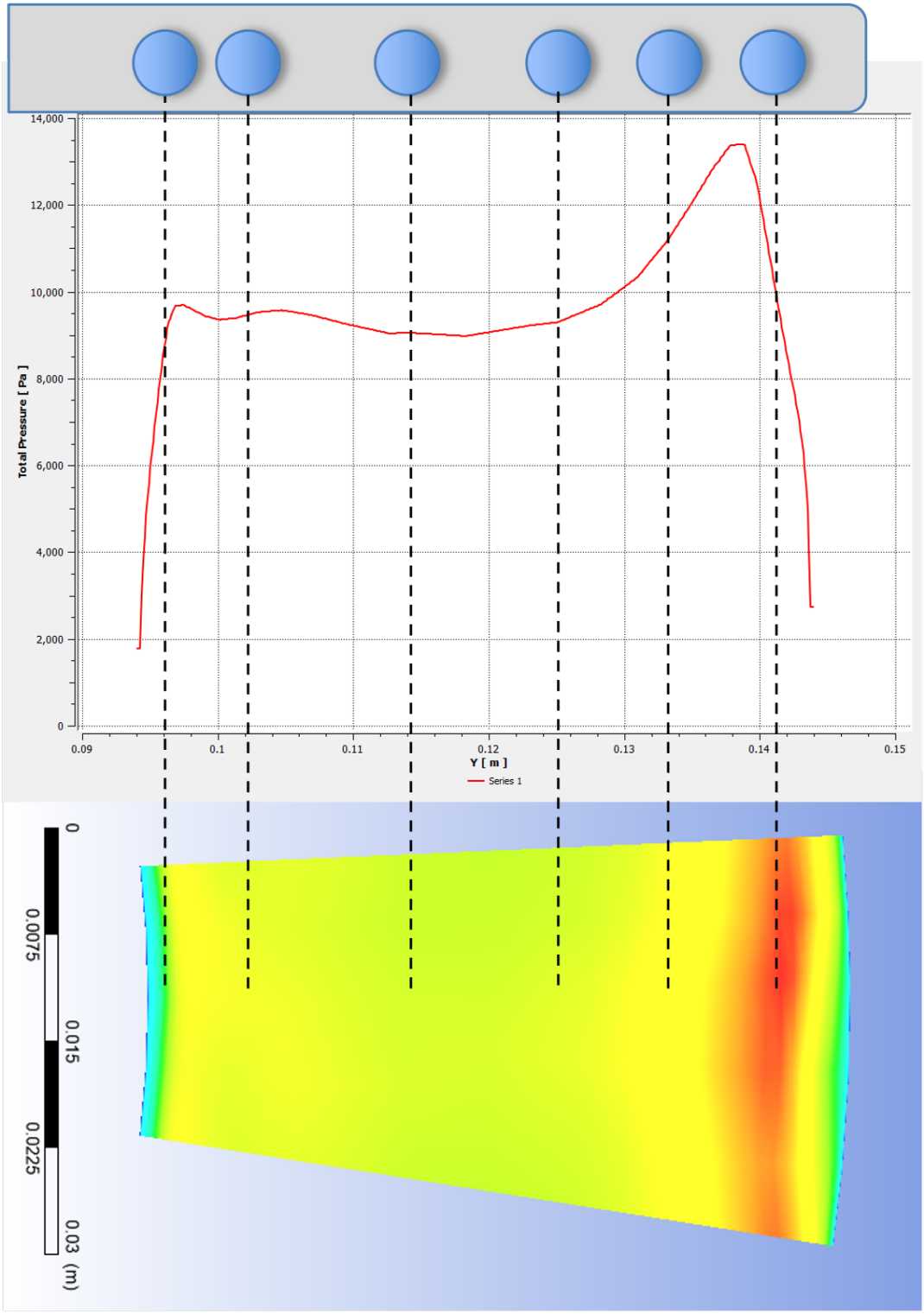


Figure 29. Plane measurements for total pressure.

# V. INSTRUMENTATION PROBE DESIGN

After completing the CFD analysis and determining the specific areas requiring measurement focus, the design process for the instrumentation probes could commence. The objective of this phase of the research was to combine the results of the CFD with the design of the DUMI to create a complete instrumentation insert that could be additively manufactured, secured to the casing, and interface with the current measurement equipment to record pressures and temperatures at different locations in the rig. As specified in the literature review, the EOS M 100 was restricted to print within a 100 mm x 100 mm x 95 mm (3.94 in x 3.94 in x 3.74 in) build size. This was one of the primary design constraints for the instrumentation probe designs.

## A. PRESSURE PROBE RAKE DESIGN

Also alluded to in the literature review, a Kiel probe design was the model for the pressure probe rake. A past conceptual design of a Kiel probe rake (Dr. Walter Smith, private communication) was used as the primary inspiration in this design process. The conceptual design used as inspiration can be seen in Figure 30.

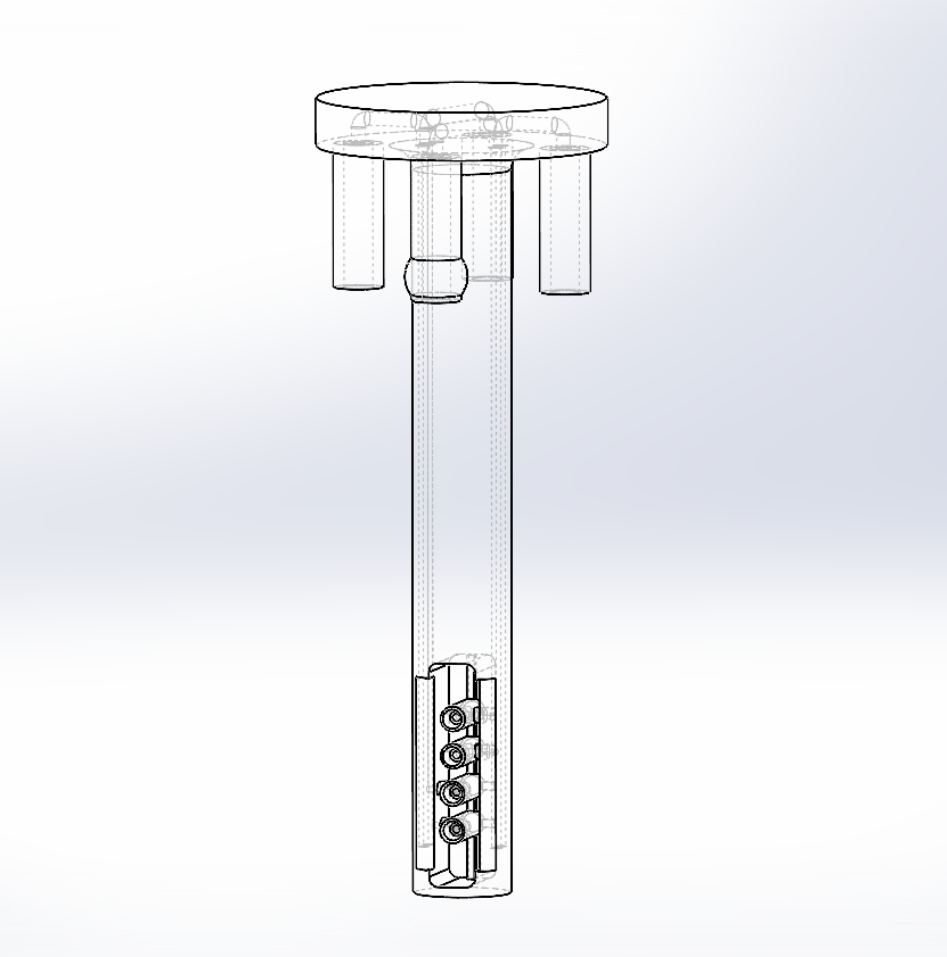

Figure 30. Base model from the TPL used as design inspiration.

Using the model, the length of the probe was made to stretch the length of the internal passage between the casing and the rotor hub. A small gap was designed between the end of the probe and the internal hub to allow for the hub to move slightly while not damaging the pressure probe. Next, the number of probe measurements in the conceptual design was increased from four to six. It was found that eight measurements would either make the thickness of the probe between gas paths too small, which would reduce the structural integrity of the probe too far, or the size of the total probe too large, which would lead to too much blockage. This improved design required two more Kiel probe shields with two more gas paths leading out the top of the probe. The locations of these measurements were parameterized as a measurement from the internal wall of the casing to the center of the shield. Instructions on how to adjust these measurement locations can

be seen in Appendix C. All that had to be known was what distribution of measurement locations would be desired. In addition to the usability of this model, some other pressure probe design benefits included that the measurements were taken on the same axial plane, there was minimal flow blockage, and the probe was structurally sound.

The final steps in designing the complete insert involved combining the pressure probe design with the DUMI and creating a gas path that would be routed out through the DUMI from the top of the pressure probe. To achieve this, the gas path cutouts on the top of the DUMI were extruded and spread out axially to create space between the gas paths. Additionally, a port was needed at the point where the gas path would exit the DUMI to connect the tubing that would link the insert to the pressure brick. The size of this port was kept consistent with the size of the ports on the current rig setup. Spreading out the gas paths reduced the interference that could be caused by the ports with tubing. A small nob was added around the port to provide a more secure attachment point for the tubing as well. Figure 31 displays the final pressure probe rake design. Figures 32 and 33 show the gas paths out from the measurement location.

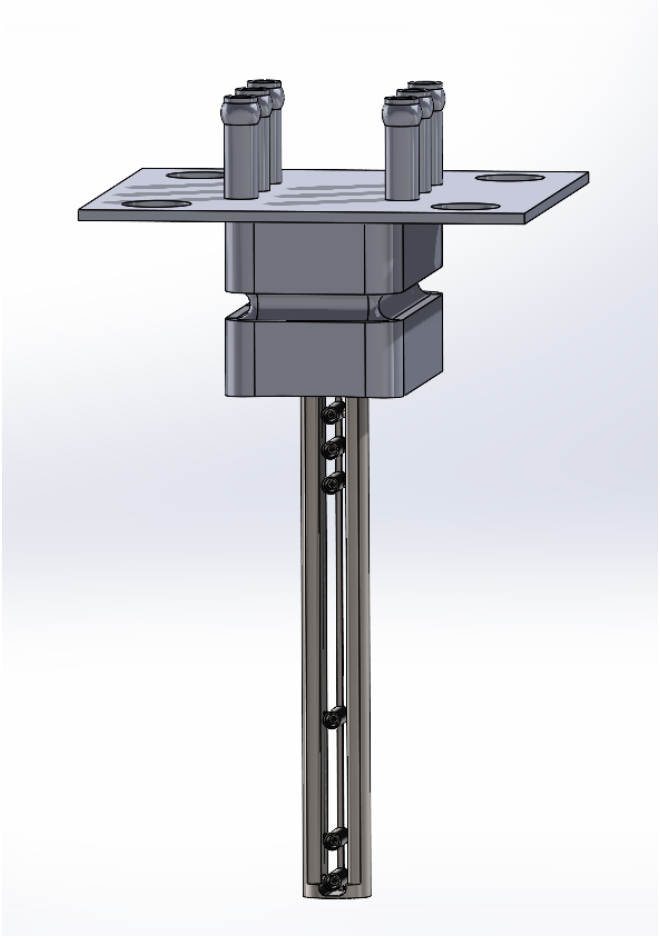

Figure 31. CAD model of the final pressure instrumentation design.

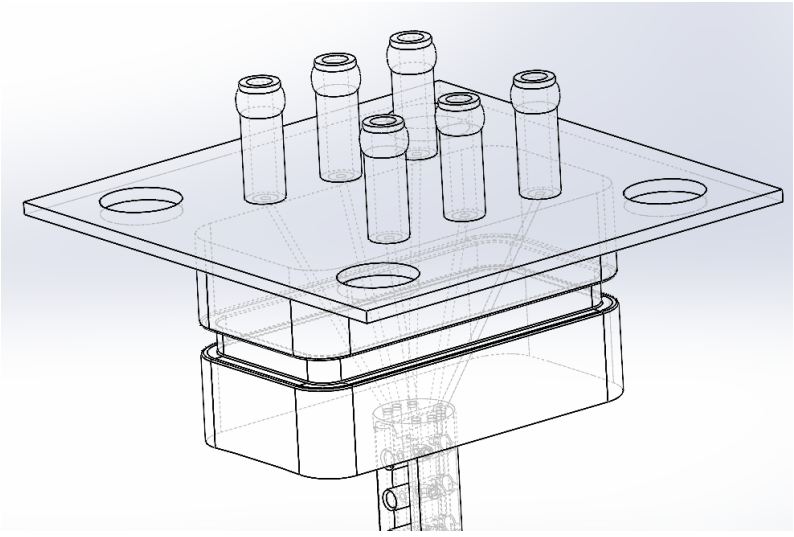

Figure 32. Gas paths routed out through the DUMI.

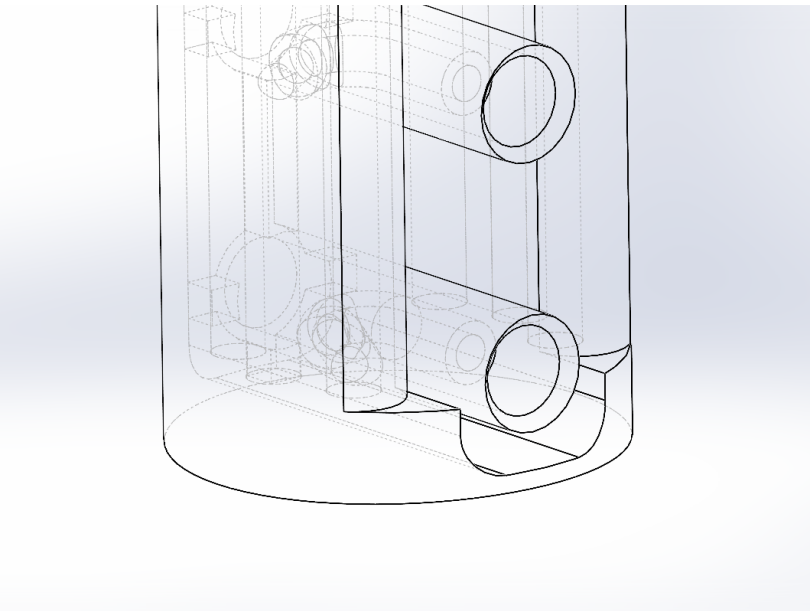

Figure 33. View of the gas paths routing out of the Kiel probe.

## B. TEMPERATURE PROBE RAKE DESIGN

The design of the temperature probe rake was somewhat simpler than the pressure probe rake as there were not multiple gas paths that had to be routed through the probe. Instead, all that was needed was a tube that a thermocouple could be threaded through and glued into place. The temperature probe design included six measurements as well to remain consistent with the pressure probe rake design.

The model was largely designed using the fundamental characteristics of the current temperature probes, which can be seen in Figures 34 and 35. The same diameter of the probe, 0.368 cm (0.145 in), was used in the new design. Next, it was found that the diameter of the desired thermocouples, as seen in the literature review in Figure 8, was 0.157 cm (0.062 in). A hole was cut out of the center of the probe to accommodate this diameter. Most of the design focus centered around the thermocouple shield.

Figure 34. Current Kiel probe/ thermocouple combination.

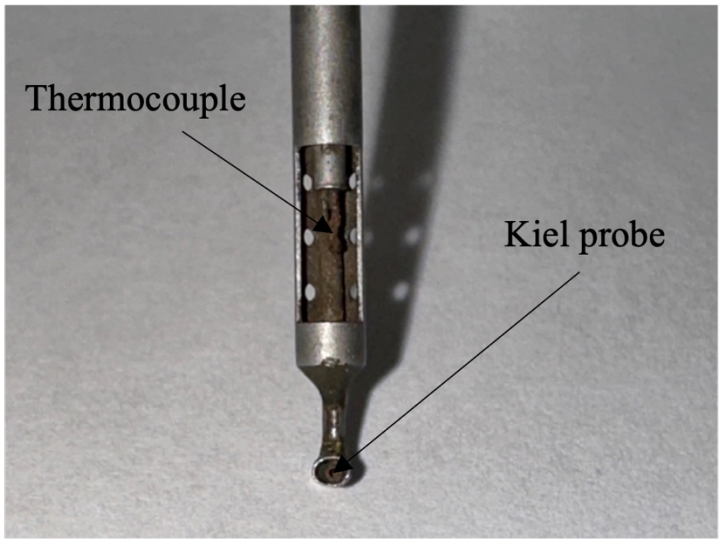


Figure 35. Close view of the Kiel probe and thermocouple.

To maximize the model's usability, the middle of the shield was parameterized within the solid modeling software, aligning it with the internal wall of the casing. The parameterization was carried out in a similar manner to the design approach for the pressure probe. Instructions on how to adjust the measurement locations of the temperature insert can be found in Appendix D. By changing this number, the middle of the shield, and the location of the thermocouple, would be set to the desired depth. The first goal of the shield design was to make the view of the shield from the front as square as possible. To do this, the inner diameter of the shield was made to be 0.254 cm (0.1 in). This would allow for a 0.572 mm (0.0225 in) wall thickness. The distance between the top and bottom surfaces of the shield were then made to be 0.254 cm (0.1 in) as well to make the frontal view of the shield square. Next, holes were placed on the backside of the shield to allow some flow to pass through which would allow for changes in temperature if the conditions of the rig were to change. The size of these holes on the new design was kept consistent with the holes on the current temperature probes which were measured to be 0.508 mm (0.02 in) in diameter.

Two more elements that were suspected to improve the performance of the probe were added to the design, and later confirmed by a CFD analysis. The first novel element regarded the number of holes on the backside of the shield. It was thought that instead of two columns of three holes on the current temperature probes, four columns of three holes would improve the measuring capabilities of the probes. The other element of the design that was introduced was a chamfer at the opening edges of the design to guide the flow towards the shield. This aspect was not included on the current temperature probes but was also thought to improve the measuring capabilities of the probes. This design was copied five more times to create a total of six measurements at different depths starting with the shallowest in front. The design can be seen in Figure 36.

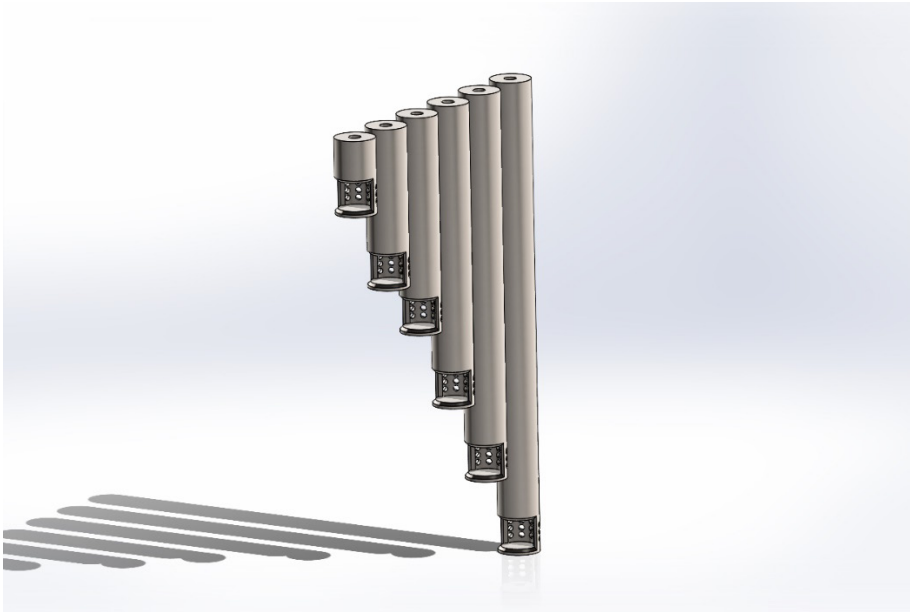

Figure 36. Arrangement of the sheaths for the thermocouples.

The biggest concern about this design was whether the flow would be diverted from the shortest probe deeper into the flow, which would cause interference between the measurement values. To ensure this was not the case, another CFD analysis was conducted. Simply put, the goal of the CFD was to confirm that this temperature probe design would not cause an interference between the six individual measurements. This was tested by introducing a flow field with a temperature gradient roughly equal to the steepest temperature gradient present in the TCR, which was 140 K across the 4.851 cm (1.91 in) gap between the inner wall of the casing and the hub at the center of the rig. The six temperature probes were placed in this flow field with a model thermocouple. The complete CFD report for this experiment can be found in Appendix E. This model thermocouple consisted of a cylinder to fill the path inside the temperature probe where a thermocouple would go with a rounded end where the measurement would be taken on a real thermocouple, as seen in Figure 37.

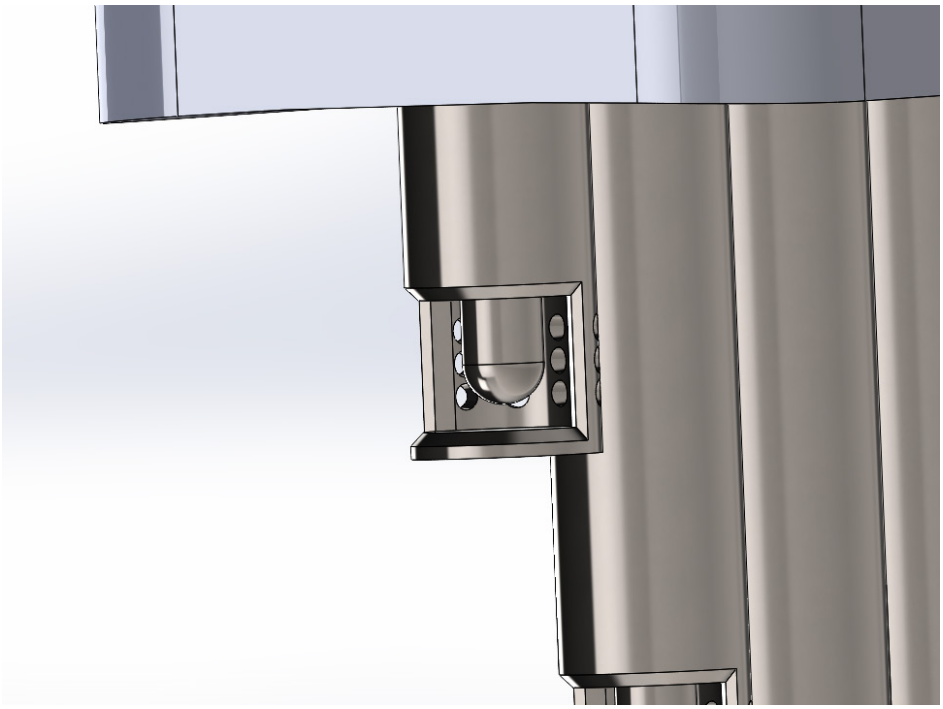

Figure 37. Close view of the sheath with model thermocouple.

Once the simulation was run, the average temperature of the surface of the exposed portion of the model thermocouple was compared to the total temperature given at the inlet for the corresponding depth. Figure 38 plots the total temperature gradient given at the inlet by radial depth in blue versus the average temperature measured by the model thermocouples in yellow at their desired measurement depths. After completing this study, it was found that the shield design described in the previous paragraph was the effective at measuring the total temperature gradient. The average temperature measured differed from the total temperature given at most 4 K with an average difference in temperature of 2.65 K. Exact differences in measurements in the CFD analysis can also be found in Appendix F.

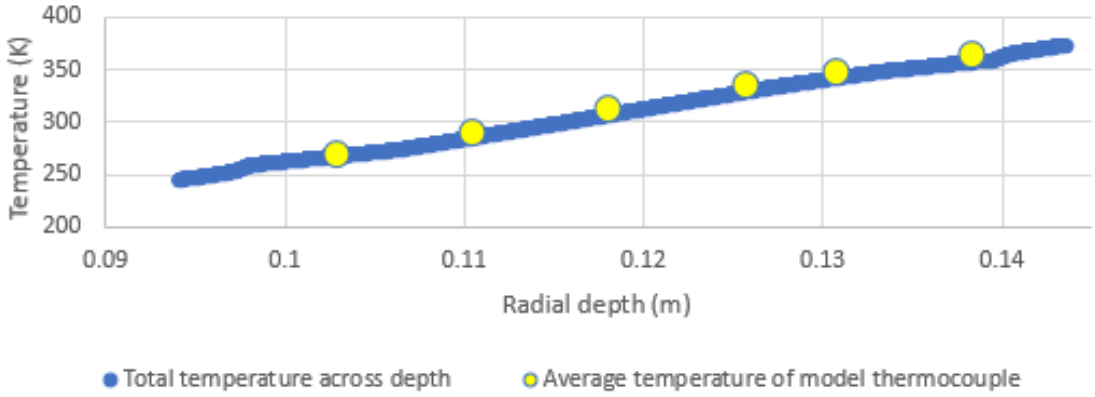


Figure 38. Plot of total temperature given versus average temperature measured by model thermocouples at various radial depths.

Similar to the pressure probe insert, once the temperature probes were designed, the next question to answer was how to route the path of the thermocouple out through the DUMI. Due to the nature of the probes, the path could be cut straight out the top of the DUMI. The main difference between the pressure and temperature inserts was the presence of the mini plug connector shown at the top of Figure 34. This connector had to secured from moving translationally or rotationally. There were two ideas about how to do this.

The first idea was to design a tripod of three posts to be printed into the top of the insert. This design incorporated a single dowel into the design to be threaded through the center of the hole in the mini plug to eliminate any translational movement. The next step was to essentially secure any yaw in the mini plug. Two more dowels were placed to allow the 0.318 cm (0.125 in) width gold connection piece between the mini plug and thermocouple wire to fit between which would eliminate any yaw from the mini plug. Each of these dowels, or posts, was designed to be 3.175 cm (1.25 in) long which would allow the 7.398 mm (0.3125 in) tall plugs to stack on top of each other. Due to the 10 cm (3.94 in) limit build height of the EOS M 100, two sets of these posts were designed each to secure three mini plugs. To eliminate any z-axis translation, a relatively heavy bolt or washer will be placed on top of the mini plugs to hold them down. Figure 39 was provided to show the design of the entire insert for reference. Figure 40 provides the hidden lines view of the same image to display the inner workings of the insert.

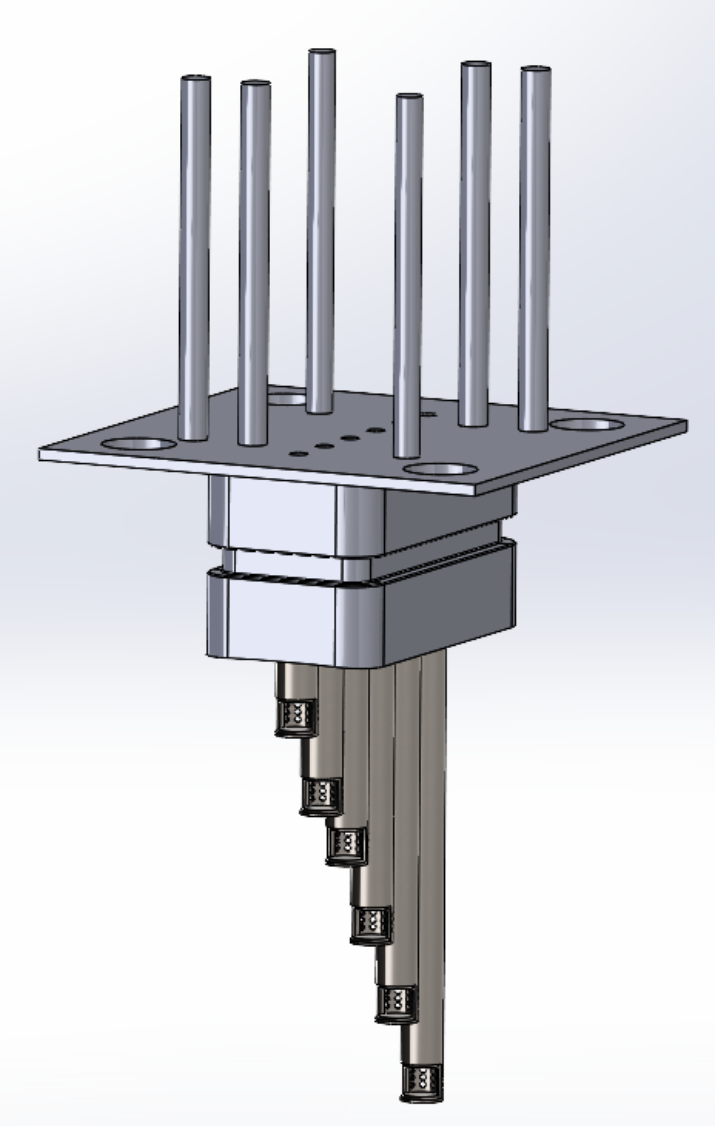

Figure 39. Upstream view of the final temperature insert design.

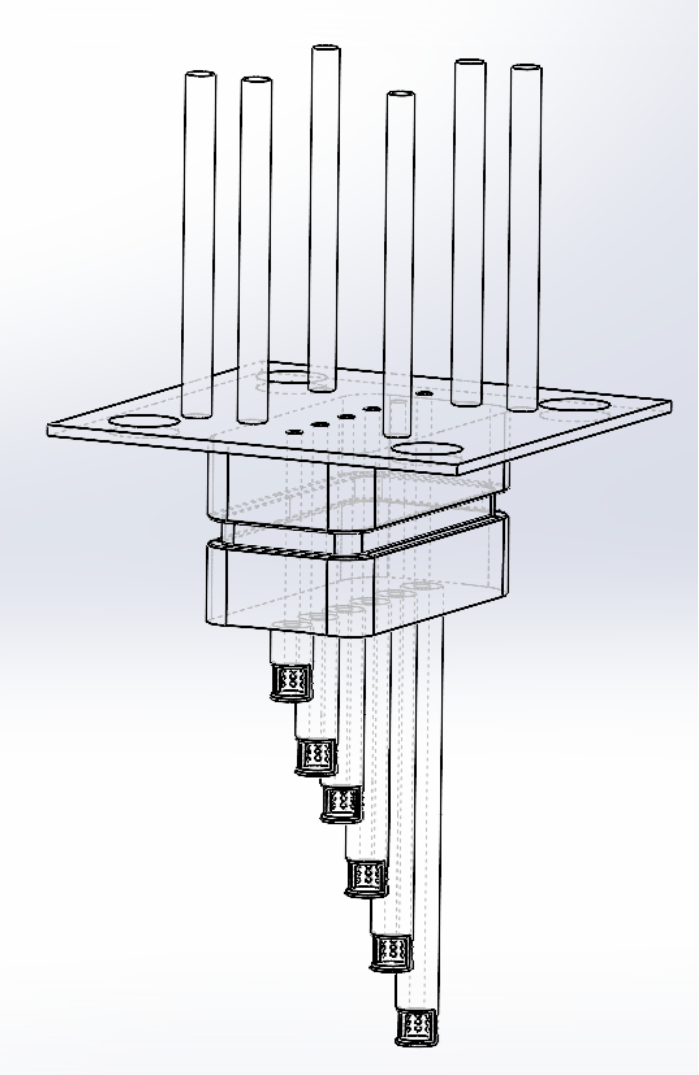

Figure 40. Hidden lines view of the final temperature insert design.

The design concept involved a separately printed body that would be secured to the casing between the screws on each datum surface and the reference surface itself. Due to the size of the mini plugs, there would have to be two of these thermocouple stress relievers per datum surface. The approach entailed constructing a 45° ramp to establish a secure resting position for the mini plug. A hole was designed into a surface at either end of the stress reliever through which a dowel could be threaded. This hole was specifically located so that the mini plug could lay down flush against the ramp and have the dowel line up

with the through holes in the stress reliever and the mini plug hole. Figure 41 displays this design.

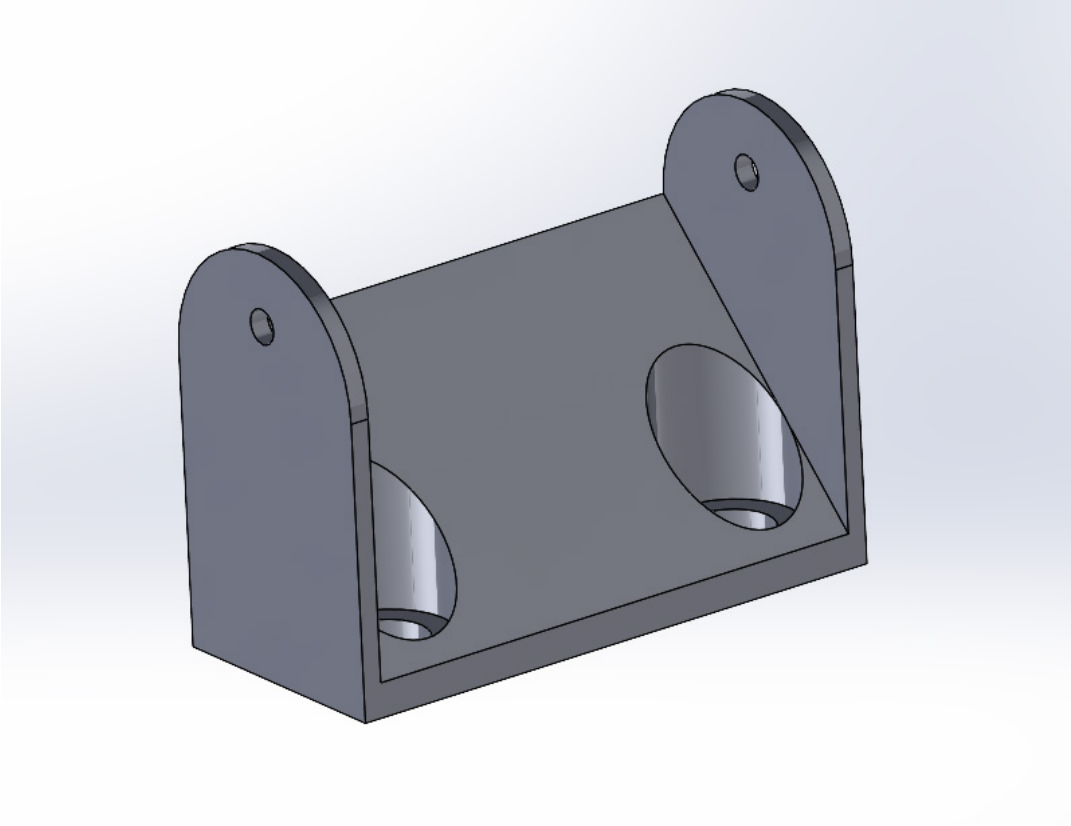

Figure 41. Mini plug stress reliever to be secured to casing.

The last step in the temperature probe design was to design a shim to act as a reference for the thermocouple to ensure the thermocouple would be glued in the right place. This device can be seen in Figure 42. The shim could be set at the bottom of the shield in a way that would introduce a surface at the desired measurement location to be glued into place. The thermocouple could then be routed down through the path in the probe until it met the reference surface of the shim and could be glued into place. Figure 43 displays how the shim is used to introduce this reference surface.

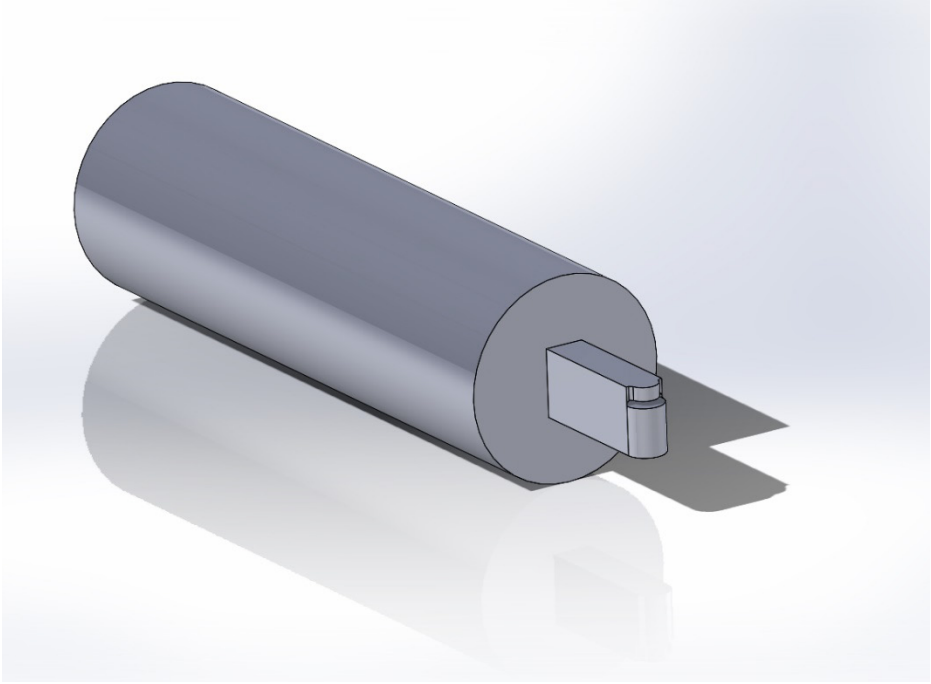

Figure 42. CAD model of the designed thermocouple positioning shim.

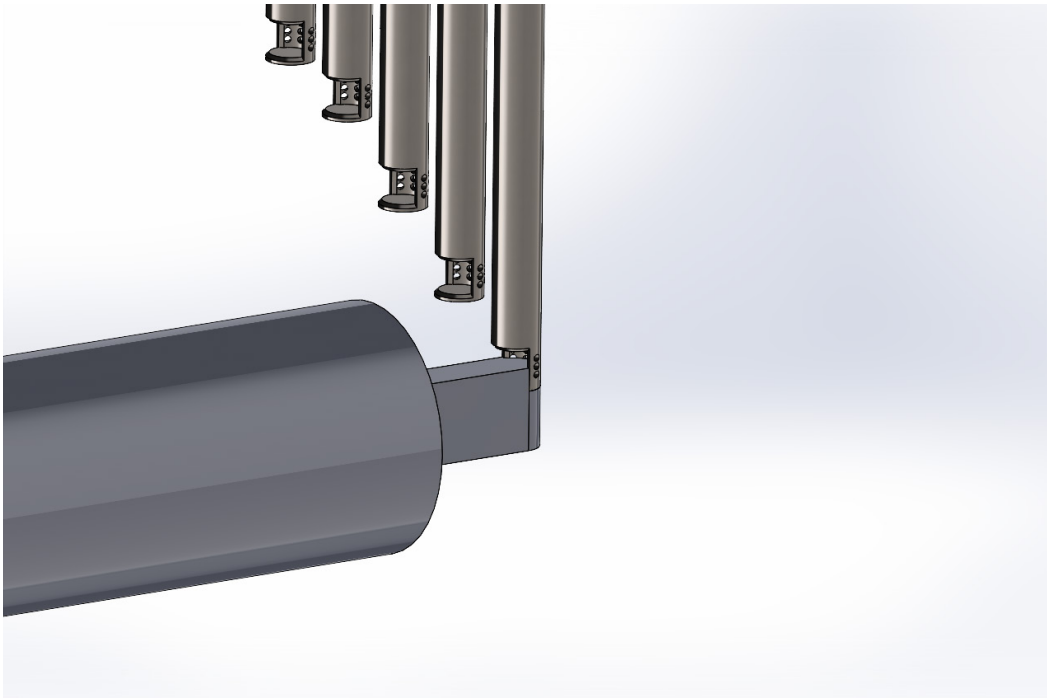

Figure 43. Example of how the shim works.

## C. MEASUREMENT LOCATION IDENTIFICATION

Once the design of the pressure and temperature inserts was complete, the distribution of measurement locations was the last aspect of the research to specify. When identifying which measurement locations were most important, the initial requirement of creating a redundant solution was kept in mind. With six pressure inserts and six temperature inserts each with six measurements, there were 36 pressure and temperature measurements designed to work with. The decision was made to create one probe to be the "redundant probe" which would provide a redundant measurement for the most desired locations, as identified from the results of the CFD analysis of the stator. It was found that 0.635 cm (0.25 in) from inside the internal wall of the instrument casing and 0.381 cm (0.15 in) away from the internal rotor hub were the locations of the peak pressures and temperatures. Knowing this, the measurement locations were clustered with a higher density around these values and evenly dispersed between peaks. The external peak was larger than the internal peak and was of greater interest. As such, each probe designated three of its measurements to map the external peak. Two of each probe's measurements were then used to map the internal peak. Lastly, each probe used one measurement to map the generally flat pressure and temperature gradient between peaks. Table 4 shows the depths, in centimeters, of each measurement with the redundant measurements highlighted in green. The same table in inches can be found in Appendix G. Figure 44 shows the dispersion of the measurement locations across the flow through the TCR with shapes corresponding to which probe each measurement belongs to identified in Table 4. In Figure 44, the y-axis is the depth into the flow. Therefore, the higher the point displayed is on the y-axis, the more internal the measurement is. The figure effectively illustrates the clustering around both peaks with less of a focus in the middle which accurately maps the pressure and temperature gradients present in the internal flow passage.

Table 4. Depths of each measurement in centimeters.

| Probe 1 (-) | Probe 2 (◆) | Probe 3 (▲) | Probe 4 (●) | Probe 5 (×) | Probe 6 (■) |
|---|---|---|---|---|---|
| 0.3048 | 0.3598 | 0.4149 | 0.4699 | 0.5249 | 0.3048 |
| 0.5800 | 0.6350 | 0.6900 | 0.7451 | 0.8001 | 0.6350 |
| 0.8551 | 0.9102 | 0.9652 | 1.0202 | 1.0753 | 0.9652 |
| 1.6030 | 2.1308 | 2.6586 | 3.1750 | 3.7028 | 3.1750 |
| 4.2418 | 4.3180 | 4.3739 | 4.4399 | 4.5060 | 4.3180 |
| 4.5720 | 4.6380 | 4.7041 | 4.7422 | 4.6990 | 4.6990 |

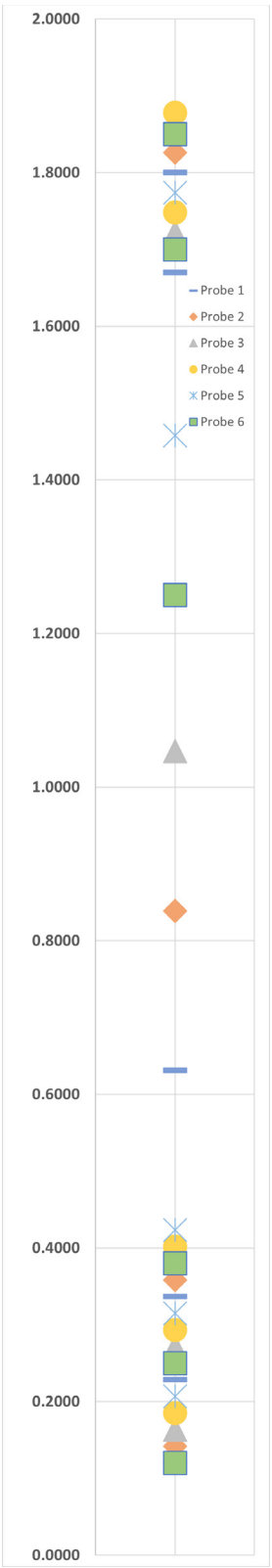


Figure 44. Visual display of the measurement distribution across the internal flow field.

THIS PAGE INTENTIONALLY LEFT BLANK

# VI. CONCLUSION

This research provided an outline of an improvement to the instrumentation on the stator casing of the Naval Postgraduate School's transonic compressor. Using initial design requirements, an entire new casing was designed according to the needs of the TPL. Next, using this newly designed casing, a new idea called a DUMI was developed to design pressure and temperature rake probes from which repeatable precise measurements could be obtained. A CFD analysis was completed on the TCR's stator for the first time. The results from this analysis provided critical information which was used to characterize the pressure and temperature instrumentation on the TCR to provide precise measurements in effective positions while introducing redundancy in the most critical positions.

At the conclusion of this thesis, the casing was in the process of being built and sent to the TPL where it could be tested and implemented on the TCR. This thesis will provide a guide to the next set of individuals to 3D print the designed inserts using the exact instructions provided in this thesis. A list of all necessary materials to add to the TCR can be found in Appendix H.

THIS PAGE INTENTIONALLY LEFT BLANK

# APPENDIX A. INSTRUMENTATION CASING AS MACHINED

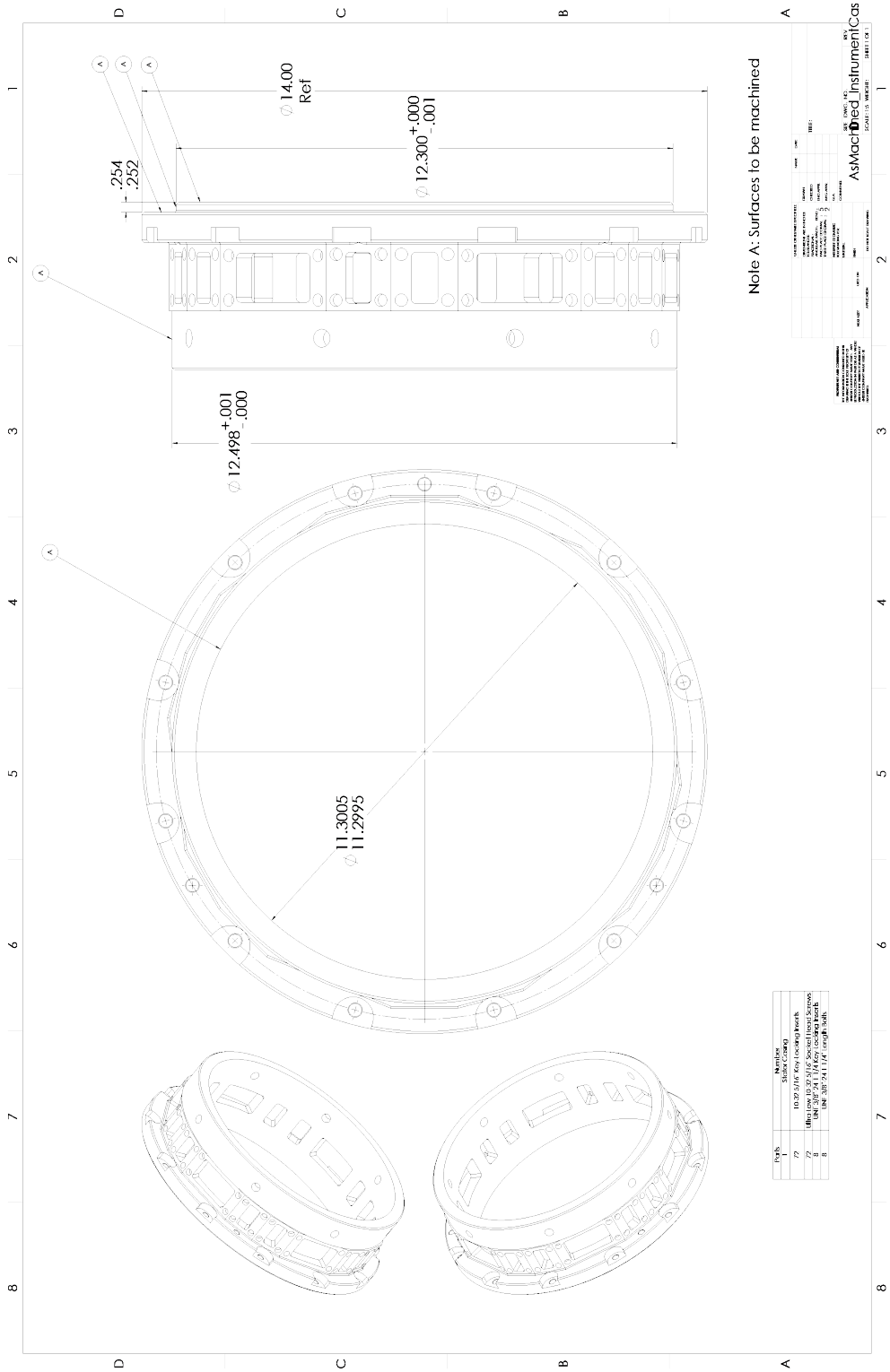

THIS PAGE INTENTIONALLY LEFT BLANK

# APPENDIX B. STATOR GAS PATH CFD REPORT


**Date**

2023/05/16 16:05:56

## Contents



## 1. File Report

**Table 1.** File Information for Copy of Fluid Flow CFX

| | |
|---|---|
| **Case** | Copy of Fluid Flow CFX |
| **File Path** | C:\Users\taylor.adams\OneDrive - Naval Postgraduate School\Downloads\ADAMS Thesis Stator Gas Path CFD_files\dp0\CFX-1\CFX\Fluid Flow CFX_002.res |
| **File Date** | 30 March 2023 |
| **File Time** | 11:56:42 AM |
| **File Type** | CFX5 |
| **File Version** | 21.2 |

## 2. Mesh Report

**Table 2.** Mesh Information for Copy of Fluid Flow CFX

| Domain | Nodes | Elements |
|---|---|---|
| Default Domain | 504472 | 1101448 |

# 3. Physics Report

**Table 3.** Domain Physics for Copy of Fluid Flow CFX

| **Domain - Default Domain** | |
|---|---|
| Type | Fluid |
| Location | B65 |
| *Materials* | |
| Air Ideal Gas | |
| Fluid Definition | Material Library |
| Morphology | Continuous Fluid |
| *Settings* | |
| Buoyancy Model | Non Buoyant |
| Domain Motion | Stationary |
| Reference Pressure | 1.0000e+0 [atm] |
| Heat Transfer Model | Total Energy |
| Include Viscous Work Term | True |
| Turbulence Model | k epsilon |
| Turbulent Wall Functions | Scalable |
| High Speed Model | Off |
| **Domain Interface - Cyclic** | |
| Boundary List1 | Cyclic Side 1 |
| Boundary List2 | Cyclic Side 2 |
| Interface Type | Fluid Fluid |
| *Settings* | |
| Interface Models | Rotational Periodicity |
| Axis Definition | Coordinate Axis |
| Rotation Axis | Coord 0.3 |
| Mesh Connection | Direct |

**Table 4.** Boundary Physics for Copy of Fluid Flow CFX

| **Domain** | **Boundaries** | |
|---|---|---|
| Default Domain | **Boundary - Inlet** | |
| | Type | INLET |
| | Location | Inlet |
| | *Settings* | |
| | Flow Regime | Subsonic |
| | Heat Transfer | Total Temperature |
| | Total Temperature | TemperatureRatio*Tinf |
| | Mass And Momentum | Cylindrical Velocity Components |

| | |
|---|---|
| Velocity Axial Component | 1.0000e+2 [m s^-1] |
| Velocity Theta Component | -7.5000e+1 [m s^-1] |
| Velocity r Component | 0.0000e+0 [m s^-1] |
| Axis Definition | Coordinate Axis |
| Rotation Axis | Coord 0.3 |
| Turbulence | Medium Intensity and Eddy Viscosity Ratio |
| **Boundary - Cyclic Side 1** | |
| Type | INTERFACE |
| Location | n11 o clock side |
| *Settings* | |
| Heat Transfer | Conservative Interface Flux |
| Mass And Momentum | Conservative Interface Flux |
| Turbulence | Conservative Interface Flux |
| **Boundary - Cyclic Side 2** | |
| Type | INTERFACE |
| Location | n1 o clock side |
| *Settings* | |
| Heat Transfer | Conservative Interface Flux |
| Mass And Momentum | Conservative Interface Flux |
| Turbulence | Conservative Interface Flux |
| **Boundary - Outlet** | |
| Type | OUTLET |
| Location | Outlet |
| *Settings* | |
| Flow Regime | Subsonic |
| Mass And Momentum | Average Static Pressure |
| Pressure Profile Blend | 5.0000e-2 |
| Relative Pressure | 0.0000e+0 [Pa] |
| Pressure Averaging | Average Over Whole Outlet |
| **Boundary - Wall** | |
| Type | WALL |
| Location | Wall |
| *Settings* | |
| Heat Transfer | Adiabatic |
| Mass And Momentum | No Slip Wall |
| Wall Roughness | Smooth Wall |

THIS PAGE INTENTIONALLY LEFT BLANK

# APPENDIX C. INSTRUCTIONS TO ADJUST PRESSURE MEASUREMENT LOCATIONS

1. Open the SolidWorks part shown below which includes only the probe named "PressureProbe." Make sure that it is not the assembly but simply the SolidWorks part.

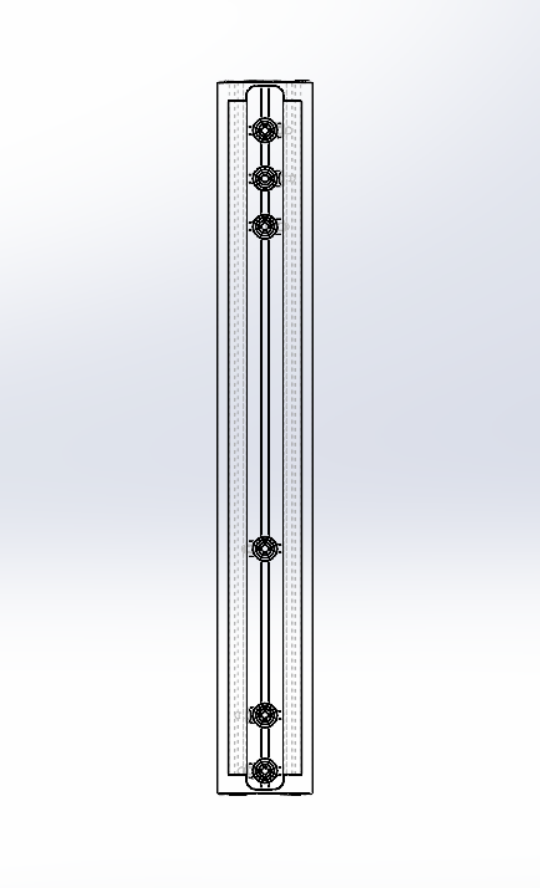

2. Open the sketch in "Boss-Extrude2" titled "Adjust here"
3. Within this sketch, there are six Smart Dimensions which measures from the interior wall of the external casing (i.e. 0.0" is located where the internal flow and the internal wall of the instrument casing meet). Adjust these six dimensions as desired by double clicking on the Smart Dimension number.
    a. Ensure the order from shallowest to deepest stays consistent

b. Ensure that the smallest number is greater than 0.0325” and the greatest number is less than 1.8675” or else the referenced geometries in SolidWorks will have conflicting messages

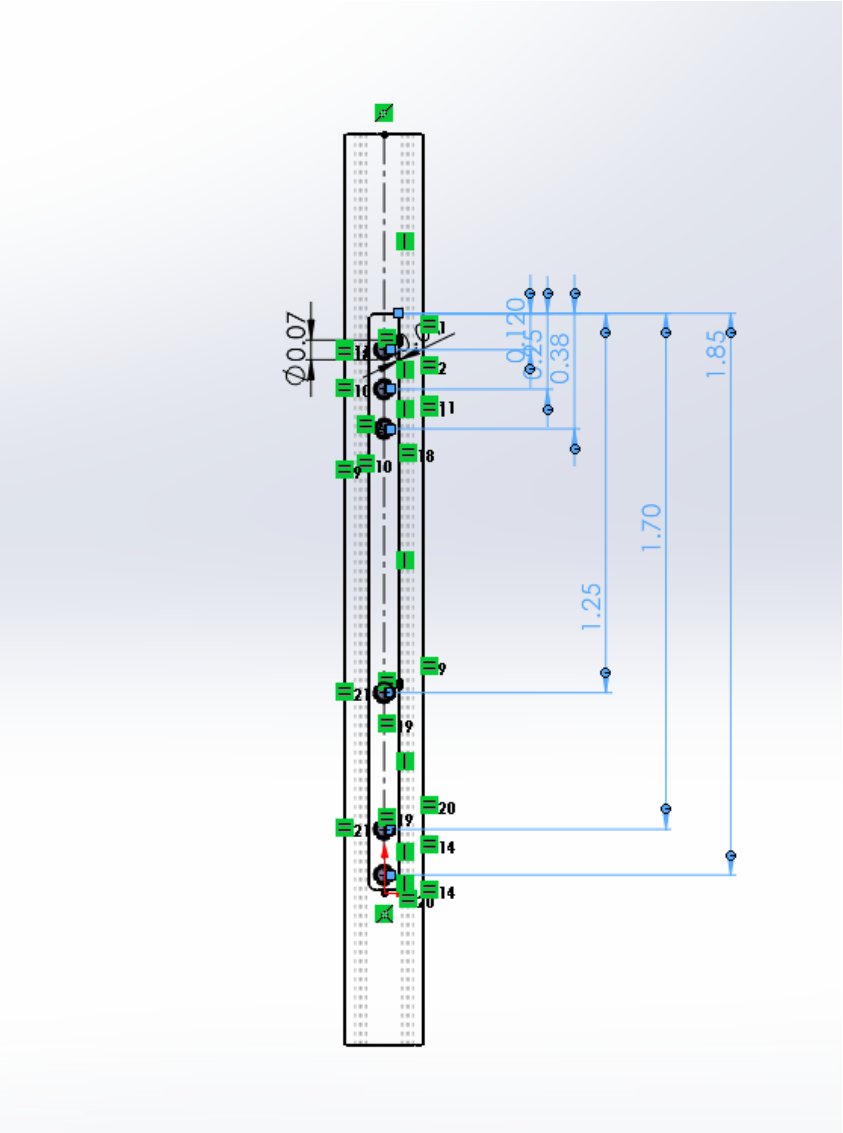


4. Lastly, simply rebuild the sketch with the updated parameters

# APPENDIX D. INSTRUCTIONS TO ADJUST TEMPERATURE MEASUREMENT LOCATIONS

1. Open the SolidWorks part shown below which includes only the probe named "TemperatureProbe."

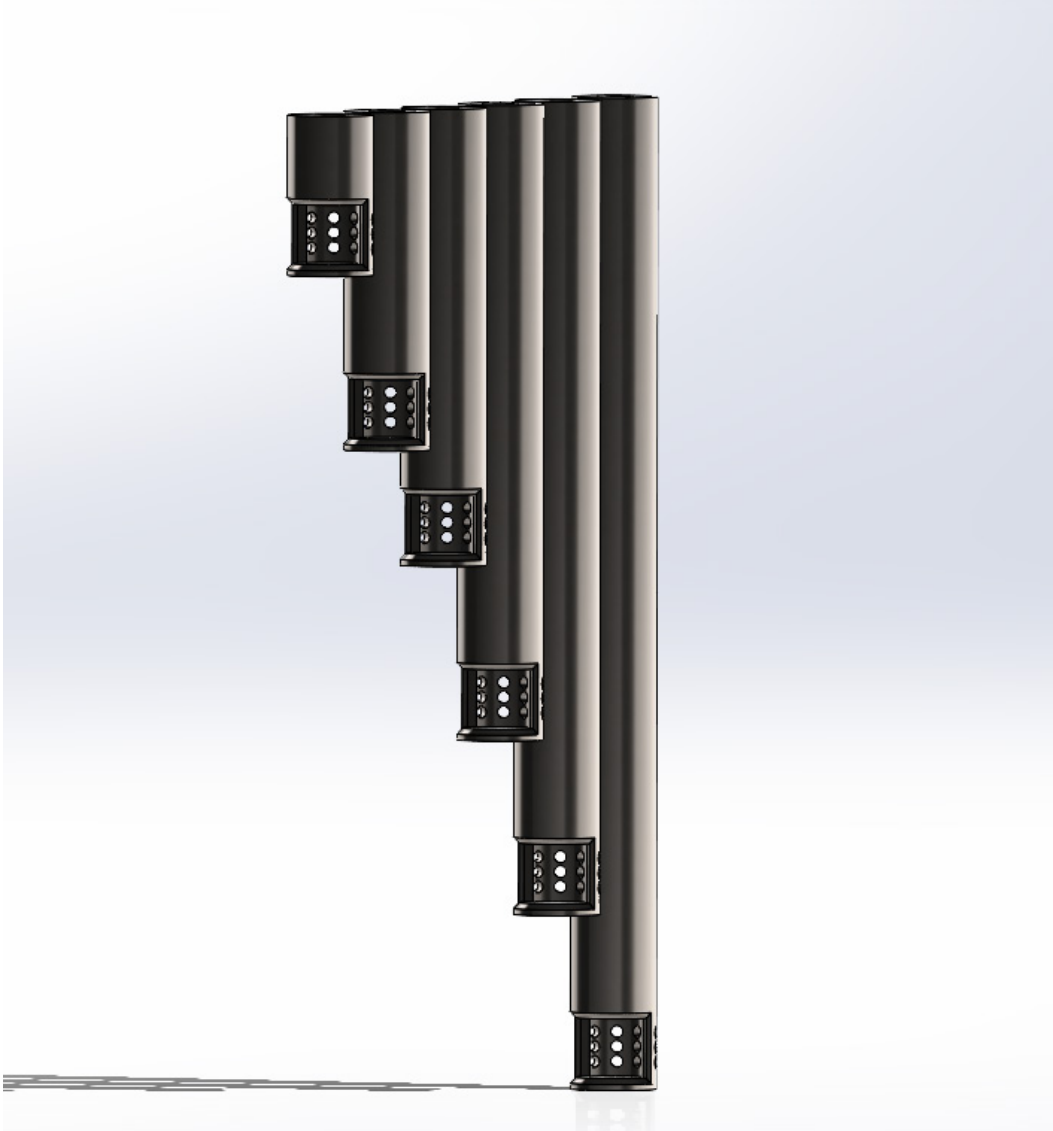

2. Open the first sketch below the origin tree item and above the measurement planes titled "Measure Depth (adjust here)"
3. Within this sketch, there are dimensions just like in the pressure probe design. Adjust these six dimensions as desired by double clicking on the Smart Dimension number.

a. Ensure the order from shallowest to deepest stays consistent
b. Ensure that the smallest number is greater than 0.06” and the greatest number is less than 1.84” or else the referenced geometries in SolidWorks will have conflicting messages

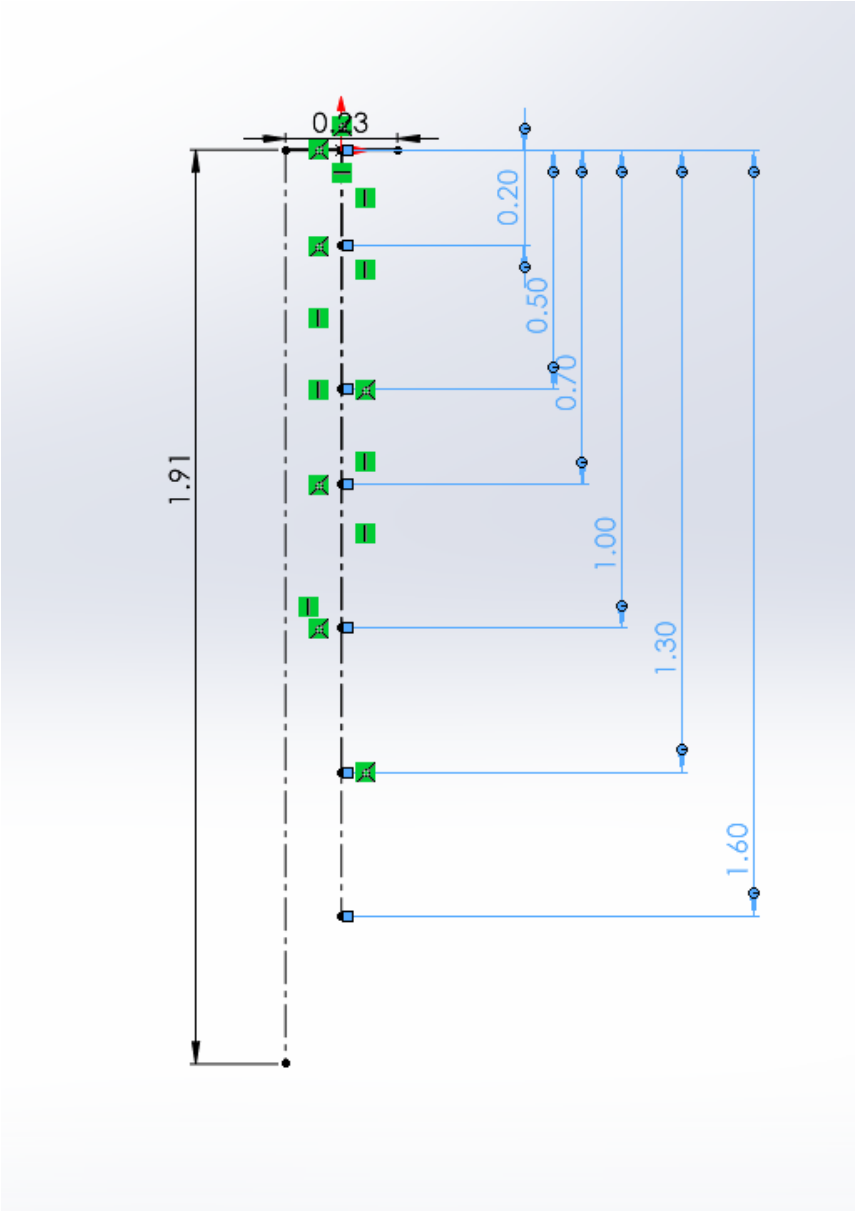


4. Lastly, simply rebuild the sketch with the updated parameters

# APPENDIX E. TEMPERATURE PROBE CFD REPORT

**Date**

2023/05/16 15:43:19

## Contents



## 1. File Report

**Table 1.** File Information for CFX

| | |
|---|---|
| **Case** | CFX |
| **File Path** | C:\Users\taylor.adams\OneDrive - Naval Postgraduate School\Downloads\ProbeConstructionCheckpoint\TemperatureProbes\BestTempProbeCFD_files\dp0\CFX\CFX\Fluid Flow CFX_005.res |
| **File Date** | 13 May 2023 |
| **File Time** | 06:11:36 PM |
| **File Type** | CFX5 |
| **File Version** | 23.1 |

## 2. Mesh Report

**Table 2.** Mesh Information for CFX

| Domain | Nodes | Elements |
|---|---|---|
| Default Domain | 166283 | 566065 |

## 3. Physics Report

**Table 3.** Domain Physics for CFX

| **Domain - Default Domain** | |
|---|---|
| Type | Fluid |
| Location | B1278 |
| *Materials* | |
| Air at 25 C | |
| Fluid Definition | Material Library |
| Morphology | Continuous Fluid |
| *Settings* | |
| Buoyancy Model | Non Buoyant |
| Domain Motion | Stationary |
| Reference Pressure | 1.0000e+0 [atm] |
| Heat Transfer Model | Total Energy |
| Include Viscous Work Term | True |
| Turbulence Model | SST |
| Turbulent Wall Functions | Automatic |
| High Speed Model | Off |

**Table 4.** Boundary Physics for CFX

| **Domain** | **Boundaries** | |
|---|---|---|
| Default Domain | **Boundary - Inlet** | |
| | Type | INLET |
| | Location | Front |
| | *Settings* | |
| | Flow Regime | Subsonic |
| | Heat Transfer | Total Temperature |
| | Total Temperature | TempProf |
| | Mass And Momentum | Normal Speed |
| | Normal Speed | 1.5000e+2 [m s^-1] |
| | Turbulence | Medium Intensity and Eddy Viscosity Ratio |
| | **Boundary - Outlet** | |
| | Type | OUTLET |
| | Location | Back |
| | *Settings* | |
| | Flow Regime | Subsonic |
| | Mass And Momentum | Average Static Pressure |
| | Pressure Profile Blend | 5.0000e-2 |
| | Relative Pressure | 0.0000e+0 [Pa] |
| | Pressure Averaging | Average Over Whole Outlet |
| | **Boundary - OtherSide** | |
| | Type | WALL |
| | Location | n1Side |
| | *Settings* | |
| | Heat Transfer | Adiabatic |
| | Mass And Momentum | Free Slip Wall |
| | **Boundary - Probe1** | |

| | |
|---|---|
| Type | WALL |
| Location | Probe1 |
| *Settings* | |
| Heat Transfer | Adiabatic |
| Mass And Momentum | No Slip Wall |
| Wall Roughness | Smooth Wall |
| **Boundary - Probe2** | |
| Type | WALL |
| Location | Probe2 |
| *Settings* | |
| Heat Transfer | Adiabatic |
| Mass And Momentum | No Slip Wall |
| Wall Roughness | Smooth Wall |
| **Boundary - Probe3** | |
| Type | WALL |
| Location | Probe3 |
| *Settings* | |
| Heat Transfer | Adiabatic |
| Mass And Momentum | No Slip Wall |
| Wall Roughness | Smooth Wall |
| **Boundary - Probe4** | |
| Type | WALL |
| Location | Probe4 |
| *Settings* | |
| Heat Transfer | Adiabatic |
| Mass And Momentum | No Slip Wall |
| Wall Roughness | Smooth Wall |
| **Boundary - Probe5** | |
| Type | WALL |
| Location | Probe5 |
| *Settings* | |
| Heat Transfer | Adiabatic |
| Mass And Momentum | No Slip Wall |
| Wall Roughness | Smooth Wall |
| **Boundary - Probe6** | |
| Type | WALL |
| Location | Probe6 |
| *Settings* | |
| Heat Transfer | Adiabatic |
| Mass And Momentum | No Slip Wall |
| Wall Roughness | Smooth Wall |
| **Boundary - Sides** | |
| Type | WALL |
| Location | n11Side |
| *Settings* | |
| Heat Transfer | Adiabatic |
| Mass And Momentum | Free Slip Wall |
| **Boundary - Wall** | |
| Type | WALL |
| Location | BottomWall, TopWall, ProbeLengths |
| *Settings* | |
| Heat Transfer | Adiabatic |
| Mass And Momentum | No Slip Wall |
| Wall Roughness | Smooth Wall |

## 4. User Data

Chart 1.

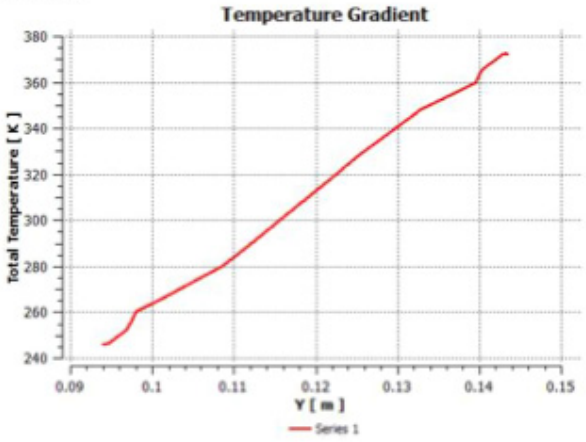

# APPENDIX F. DIFFERENCE IN EXPECTED VERSUS MEASURED TEMPERATURES IN TEMPERATURE PROBE CFD EXPERIMENT

| Depth from center of rig (m) | 0.13843 | 0.130816 | 0.125735 | 0.118119 | 0.110498 | 0.102881 |
|---|---|---|---|---|---|---|
| Avg temp measured (K) | 361.715 | 345.319 | 332.862 | 310.836 | 287.68 | 267.935 |
| Total temp given (K) | 357.6615 | 342.5872 | 329.374 | 307.3989 | 285.6192 | 267.7978 |
| Difference | 4.053463 | 2.73179 | 3.487978 | 3.437132 | 2.060814 | 0.137172 |

THIS PAGE INTENTIONALLY LEFT BLANK

# APPENDIX G. PROBE MEASUREMENT LOCATIONS IN INCHES

| Probe 1 (-) | Probe 2 (◆) | Probe 3 (▲) | Probe 4 (●) | Probe 5 (×) | Probe 6 (■) |
|---|---|---|---|---|---|
| 0.1200 | 0.1417 | 0.1633 | 0.1850 | 0.2067 | 0.1200 |
| 0.2283 | 0.2500 | 0.2717 | 0.2933 | 0.3150 | 0.2500 |
| 0.3367 | 0.3583 | 0.3800 | 0.4017 | 0.4233 | 0.3800 |
| 0.6311 | 0.8389 | 1.0467 | 1.2500 | 1.4578 | 1.2500 |
| 1.6700 | 1.7000 | 1.7220 | 1.7480 | 1.7740 | 1.7000 |
| 1.8000 | 1.8260 | 1.8520 | 1.8670 | 1.8500 | 1.8500 |

THIS PAGE INTENTIONALLY LEFT BLANK

# APPENDIX H. LIST OF MATERIALS AND TOOLS NEEDED FOR THE TCR INSTRUMENTATION OPTIMIZATION

| Number | Item |
|---|---|
| 72 | 90357A132_Ultra-Low-Profile Socket Head Screws |
| 72 | 93340A305_18-8 Stainless Steel Key-Locking Inserts |
| 12 | 91271a585 Alloy-Steel 12-Point Screw, 5/16”-18 Thread Size, 1–1/4” Long |
| 8 | 91251A426 Black-Oxide Alloy Steel Socket Head Screw, 3/8”-24 Thread Size, 1–1/4” Long |
| 8 | 93340A320 18–8 Stainless Steel Key-Locking Inserts with Thin Wall, 3/8”-24 Thread Size |
| 1 | 5125A2 Ratcheting Combination Wrench, Horizontal Flex-Head, 5/16” Size, 5” Overall Length |

THIS PAGE INTENTIONALLY LEFT BLANK

# LIST OF REFERENCES


[1] D. McNab, "Experimental Testing and CFD Modeling of an Advanced Transonic Compressor for Military Applications," M.S. thesis, Dept. of Mechanical and Aerospace Engineering, Naval Postgraduate School, Monterey, CA, 2011.

[2] S. Drayton, "Design, Test, and Evaluation of a Transonic Axial Compressor Rotor with Splitter Blades," Ph.D. dissertation, Dept. of Mechanical and Aerospace Engineering, Naval Postgraduate School, Monterey, CA, 2013.

[3] T. D. Belna, "Upgrade Transonic Compressor Test Rig Data Acquisition System," M.S. thesis, Dept. of Mechanical and Aerospace Engineering, Naval Postgraduate School, Monterey, CA, 2018.

[4] E. Bach et al., "Kiel Probes for Stagnation Pressure Measurement in Rotating Detonation Combustors," AIAA J., vol. 60, no. 6, pp. 3724–3735, Jun. 2022, doi: 10.2514/1.J061061.

[5] A. Lejdeby, "Design and Calibration of Pneumatic Probes for Aerodynamic Testing," M.S. thesis, KTH, Stockholm, Sweeden, 2021.

[6] M. K. Oldfield, A. Castillo Pardo, and C. A. Hall, "Fan Stability Enhancement With Partial Casing Treatments," J. Turbomach., vol. 144, no. 12, Sep. 2022, doi: 10.1115/1.4055386.

[7] D. D. Pollock, "Introduction," in *Thermocouples: Theory and Properties*. Boca Raton, FL, USA, CRC Press, 1991, ch. 1, pp. 1–2.

[8] Omega Engineering, Inc., "Working principle of thermocouples." omega.com [Online]. Available: https://www.omega.com/en-us/resources/how-thermocouples-work (accessed May 05, 2023).

[9] P. H. Hearn, "Transonic Compressor Inlet Flow Field Analysis." M.S. thesis, Dept. of Mechanical and Aerospace Engineering, Naval Postgraduate School, Monterey, CA, 2021.

[10] F. Durst, A. Melling, and J. H. Whitelaw, *Principles and Practice of Laser-Doppler Anemometry*, 2nd ed. London ; New York: Academic Press, 1981, ch. 1, pp. 1–4.

[11] Advanced Thermal Solutions, Inc.. "Understanding Hot-Wire Anemometry." mouser.com [Online]. Available: https://www.mouser.com/catalog/additional/ATS_Qpedia_Dec07_Understanding%20hot%20wire%20amemometry9.pdf (accessed May 05, 2023).

[12] R. Maury, A. Strzelecki, Y. Lehot, and J. Vallet, "Alternative Method to LNG Flowrate Measurement," presented at the LGN 18 Conference, Perth, Australia, Apr. 2016.

[13] J. D. Anderson Jr. et al., "Basic Philosophy of CFD" in *Computational Fluid Dynamics: An Introduction*, 3rd ed. Berlin, Germany, Springer Science & Business Media, 2008, ch. 1, pp. 3–14.

[14] S. Adekanye, R. Mahamood, E. Akinlabi, and G. Owolabi, "Additive Manufacturing: The Future of Manufacturing," *Mater. Tehnol.*, vol. 51, no. 5, pp. 709–715, Oct. 2017, doi: 10.17222/mit.2016.261.

[15] A. B. Acél, G. Falk, F. Dömötör, and J. Takács, "Design and Quality Assured Manufacturing of Free Form Metal Prostheses by Selective Laser Melting Technology," Hung. J. Ind. Chem., vol. 49, no. 2, pp. 29–34, 2021.

[16] Pick 3D Printer, "EOS M100 3D Printer In-Depth Review," pick3dprinter.com, Jan. 16, 2021 [Online]. Available: https://pick3dprinter.com/eos-m100-review/ (accessed May 05, 2023).

[17] 3Dnatives, "EOS M 100," 3dnatives.com [Online]. Available: https://www.3dnatives.com/3D-compare/en/3d-printers/eos-m-100/ (accessed May 05, 2023).

[18] Global O-Ring and Seal, LLC, "O-Ring Groove Design," globaloring.com [Online]. Available: https://www.globaloring.com/o-ring-groove-design/ (accessed May 11, 2023).

[19] N. J. Spector, "Manufacturing Methods, Experimental, and Computational Analysis of Ducted Flow Control Devices in a Transonic Compressor." M.S. thesis, Dept. of Mechanical and Aerospace Engineering, Naval Postgraduate School, Monterey, CA, 2023.

# INITIAL DISTRIBUTION LIST

1. Defense Technical Information Center
   Ft. Belvoir, Virginia

2. Dudley Knox Library
   Naval Postgraduate School
   Monterey, California